GEOLOGOS

Mantle rock exposures at oceanic core complexes along mid-ocean ridges

Jakub Ciazela[1,2*], Juergen Koepke[2], Henry J.B. Dick[3] & Andrzej Muszynski[1]

[1]Institute of Geology, Adam Mickiewicz University, Institute of Geology, Maków polnych 16, 61-606 Poznań, Poland
[2]Institut für Mineralogie, Leibniz Universität Hannover, Callinstrasse 3, 30167 Hannover, Germany
[3]Department of Geology and Geophysics, Woods Hole Oceanographic Institution, MS #8, McLean Laboratory, Woods Hole MA 02543-1539, USA
* corresponding author, e-mail: ciazela@amu.edu.pl

Abstract

The mantle is the most voluminous part of the Earth. However, mantle petrologists usually have to rely on indirect geophysical methods or on material found ex situ. In this review paper, we point out the in-situ existence of oceanic core complexes (OCCs), which provide large exposures of mantle and lower crustal rocks on the seafloor on detachment fault footwalls at slow-spreading ridges. OCCs are a common structure in oceanic crust architecture of slow-spreading ridges. At least 172 OCCs have been identified so far and we can expect to discover hundreds of new OCCs as more detailed mapping takes place. Thirty-two of the thirty-nine OCCs that have been sampled to date contain peridotites. Moreover, peridotites dominate in the plutonic footwall of 77% of OCCs. Massive OCC peridotites come from the very top of the melting column beneath ocean ridges. They are typically spinel harzburgites and show 11.3–18.3% partial melting, generally representing a maximum degree of melting along a segment. Another key feature is the lower frequency of plagioclase-bearing peridotites in the mantle rocks and the lower abundance of plagioclase in the plagioclase-bearing peridotites in comparison to transform peridotites. The presence of plagioclase is usually linked to impregnation with late-stage melt. Based on the above, OCC peridotites away from segment ends and transforms can be treated as a new class of abyssal peridotites that differ from transform peridotites by a higher degree of partial melting and lower interaction with subsequent transient melt.

Keywords: peridotite, OCC, detachment fault, megamullion, slow-spreading ridge

1. Introduction

The mantle is the most voluminous part of the Earth. Assuming that the Earth's core has a radius of 3,482 km (Dziewonski & Anderson, 1981) and that the average depth to the Moho is 26.4 km (Bagherbandi et al., 2013). It can be concluded that the mantle constitutes 82.4% of the volume of the Earth. Therefore, it is crucial to understand its structure, heterogeneities and bulk composition, in order to infer the composition of the bulk Earth. The composition of the mantle, compared to that of the bulk Earth, can be used to estimate the composition of the Earth's core (Carlson, 2003). Moreover, the mantle plays an important role in our understanding of the mechanisms of plate tectonics (Morris & Ryan, 2003) and the accretion of oceanic and continental crust (e.g., Kelemen et al., 1997; Martinez & Taylor, 2002). Another important aspect is related to the giant mass of water that is contained in the mantle. There are 1.5×10^{24} g of water on the Earth's surface (mainly oceans), which corresponds to 250 ppm of the Earth's bulk composition. At least half of that is thought to be found in the mantle, which is the main deep water reservoir in the Earth system. Some researchers estimate that the mantle might contain even 10 times the quantity of water in the ocean (Marty &Yokochi, 2006). Finally, the

mantle might be an important reservoir of hydro-carbons (Scott et al., 2004), as suspected already by Gold (1999) in his controversial book *The deep hot biosphere*. In fact, the biosphere may exist in suboceanic mantle according to the newest research (Menez et al., 2012; McCollom & Seewald, 2013).

For all these reasons, the great interest in the composition of the Earth's mantle is not surprising. In the present paper, we review the commonest sources of our knowledge of the mantle (Section 2) and provide a new data set for abyssal mantle rocks that is available due to the discovery of oceanic core complexes (OCCs). We describe the typical tectonic settings of OCCs (Section 3), the general mechanism of their emplacement and classify them according to spreading rate and magma flux (Section 4). Subsequently, we list all OCCs discovered so far (Section 5) and focus on those that contain greater amounts of mantle rocks (Section 6). Finally, we discuss their origin and petrological aspects and conclude that they exhibit special characteristics that potentially distinguish them from abyssal peridotites formed in other geotectonic settings.

2. Traditional sources of our knowledge of the mantle

The deepest Earth samples recovered so far are preserved in diamonds; they are possibly derived from the top of the lower mantle. However, although they came from the ultra-deep mantle, they probably represent an anomalous composition, due to the special conditions related to diamond formation. Mantle rocks delivered to the Earth's surface as xenoliths in basaltic magmas are quite common. However, these are also limited in size and do not provide information on field relations. Furthermore, they are often influenced by the infiltrating host magma. Nevertheless, they do represent almost the whole upper mantle, since some xenoliths found in kimberlites come from a depth of 500 km near the transition zone between the upper and lower mantle (Pearson et al., 2003).

Only the uppermost mantle is represented by orogenic, ophiolitic and abyssal peridotites. All three types are often strongly altered. However, those that are sufficiently well preserved, reveal unique information about the structural relationship between different lithologies, the melt extraction from the mantle source, melt flow in lithospheric vein conduits (Bodinier & Godard, 2003) and the mantle flow beneath a ridge (Jousselin et al., 1998). Abyssal peridotites yield the most complete

information about the mantle below the oceanic crust, which is sparsely sampled by xenoliths. Most occurrences of abyssal peridotites are found at mid-ocean ridges. The few other locations where they have been recognised include passive margins and supra-subduction zones (Bodinier & Godard, 2003; Parkinson & Pearce, 1998), with the most intensely investigated ones situated in the Parece Vela Basin (Ohara et al., 2003b).

3. Slow-spreading ridges as a suitable tectonic setting for OCC

There is far more potential for mantle rocks to be exposed at slow-spreading ridges compared to fast-spreading ones. In a review paper, Bodinier & Godard (2003) listed only three such localities at fast-spreading ridges: at Hess deep and at Garret and Terevaka Fracture Zones to the south of Hess deep. The scarcity of peridotites at fast-spreading ridges results from the relatively high crustal thickness along fast-spreading ridges (~7 km; White et al., 1992; Canales et al., 1998, 2003) and the regular sequence of basaltic carapace (1–2 km), sheeted dykes (1–2 km) and gabbros (3–5 km) (Klein, 2003); see Fig. 1A. It was believed for a long time that this model of the crust was also valid for slow-spreading ridges, as was proposed by Penrose Conference Participants (1972). However, when we observe the topography of the two kinds of ridges, we notice that the surface of the fast-spreading ridge area is usually smooth compared to slow-spreading ridges, with no median valley, while the surface of the slow-spreading ridges area is rugged with kilometre-scale relief and a deep 1–2 km median valley at the spreading axis (Wilson, 1997). This discrepancy is related to the lower and more episodic flux of magma and thicker lithosphere in slow-spreading ridges (Macdonald et al., 1993). The latter results in considerable heterogeneity of the crust (Dick et al., 2006). Dick (1989) reported a decrease of crustal thickness with distance from the segment centre at slow-spreading ridges (Fig. 1B). Cannat (1996) proposed a model of a very heterogeneous crust similar to a "plum-pudding", in which gabbro bodies are dispersed in peridotite mantle (Fig. 1C), which contrasts strongly with the model of a homogeneous, layered crust from fast-spreading ridges. Gabbro bodies predominate during high magma flux periods, and peridotites do so in magma starvation periods (see Coogan, 2013 for details). Based on the ratio of mafic rocks to mantle rock, which can be interpreted as a proxy for magma flux, Dick

Ocean Ridge Crustal Accretion Models
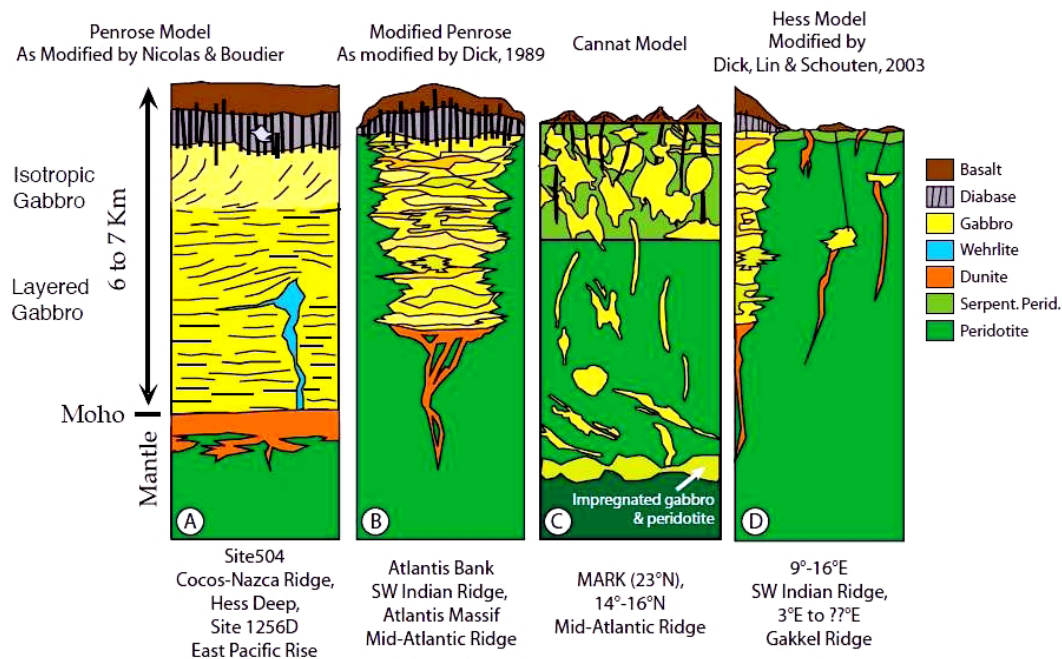
Fig. 1. Models for crustal accretion at ocean ridges. **A –** Classic interpretation of the Penrose Model for a fast-spreading ridge, as based on the Oman Ophiolite; **B –** Penrose model, as modified for slow-spreading ridges based on the abundance of peridotite and frequent absence of gabbro at transforms following focused melt-flow models; **C –** Model of the anomalous 14–16°N area of the Mid-Atlantic Ridge; **D –** Model of the magmatic and amagmatic accretionary segments at ultraslow-spreading ridges (after Dick et al., 2006)

et al. (2003) presented general models for the variety of structural types observed at slow-spreading ridges. As a new type, these authors defined ultraslow-spreading ridges (e.g., Gakkel Ridge, Southwest Indian Ridge (SWIR)), which are characterised by very low magma flux. Here, the scarcity of gabbro bodies in some regions results in the absolute predominance of peridotites just below a thin, irregular basaltic carapace and sedimentary cover (Fig. 1D).

For a long time, abyssal peridotites were recovered only at deep axial valleys, transform faults and fracture zones, where lower crustal and mantle rocks are tectonically exposed on their walls
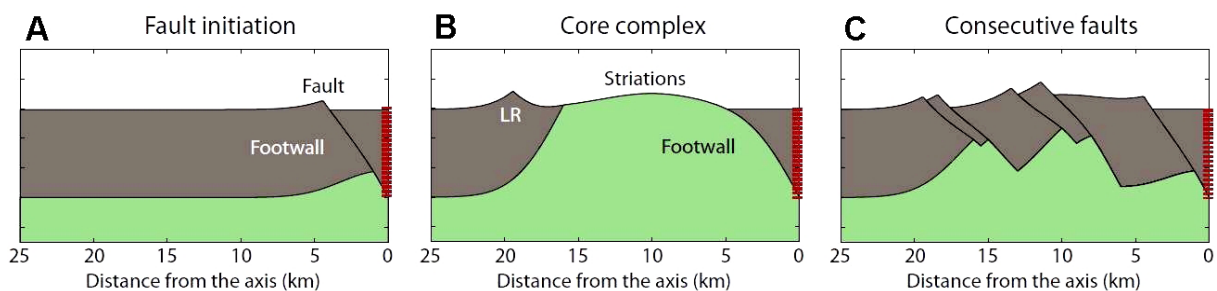
Fig. 2. Two styles of faulting at a slow-spreading ridge. Faults are indicated as subsurface black lines, and the footwall is marked. A normal fault forms, dipping at 60° beneath the axis. **A –** In this panel, fault offset is 1 km, and the fault block has rotated outwardly away from the ridge axis by 18° to form an outward-facing scarp; **B –** Continued faulting and extension brings lower crustal rocks to the sea floor and forms a "core complex". In this panel, the fault offset is 16 km, and outward rotation of the top of the fault has increased to 36° to create a narrow linear ridge (LR) marking the breakaway where the fault initially formed. The exposed footwall may be striated; **C –** In this panel, no long-lived faults have formed. Instead, consecutive short-lived faults cut the lithosphere on the ridge flank to form classic abyssal hill topography.

Red dashed line – spreading axis. Brown shading – crust that predates faulting. Green shading – material below the crust that is brought to the surface during core-complex formation (after Smith et al., 2012).

(Dick, 1989; Cannat et al., 1993). These outcrops are usually limited to a narrow linear zone along the walls. Although larger two-dimensional exposures of mantle and plutonic rocks were first discovered exposed by detachment faulting at ridge-transform intersections over 30 years ago (Dick et al., 1981), the majority of the geological community thought such exposures were anomalies. This changed in the mid-1990s when detachment faults were widely documented along the Mid-Atlantic Ridge (e.g., Tucholke & Lin, 1994; Tucholke et al. 1996; Cann et al., 1997). The lower parts of detachment fault footwalls represent continuous exposure of lower crust and mantle rocks on a single fault for up to millions of years and are called oceanic core complexes (OCC), due to an analogy with land core complexes that similarly exposed lower crustal rocks (Smith et al., 2012).

4. Mechanism of emplacement, features and classification of oceanic core complexes

It was believed for a long time that oceanic crust at slow-spreading ridges accreted symmetrically (e.g., Skinner et al., 2004), and that the divergent transport of the adjacent tectonic plates was mostly accommodated by the delivery of new magma (Solomon et al., 1988). In this model, periods of magma starvation are short and accommodated by short-lived, high-angle normal faults (see Fig. 2C; Thatcher & Hill, 1995; Smith et al., 2012). However, the numerous core complexes discovered on slow-spreading ridges have led to an alternative asymmetric spreading model of crustal accretion (Escartín et al., 2008). Asymmetric spreading has been interpreted as a consequence of the amount of magma flux where the proportion of magmatic extension is limited to ~30–50% relative to tectonic accretion (Tucholke et al., 2008). During periods of magma starvation, the normal fault needs to accommodate the absence of new material. In the case of a permanent starvation, it becomes a long-lived, low-angle fault (Dick et al., 1981; Tucholke et al., 1996). The fault offset represents a load which must be isostatically compensated. The lower part of the exposed footwall has a higher load deficit and moves upwards faster than the higher part. As a consequence, the detachment surface bends and eventually even past horizontal. This horizontal plane continues to move up which leads to doming of the footwall, due to the rigidity of the crust (Fig. 2). As a result, rocks of the lower plate (consisting of

the lower crust and upper mantle) can be exposed at the surface (see Fig. 2B; Buck, 1988; Lavier et al., 1999). This part of the detachment fault system creates the oceanic core complex (OCC). Fully developed OCCs occur when a given detachment is active for a sufficiently long period of time (>1 Ma; Blackman et al., 2008).

Two prominent morphological characteristics of OCCs are the domal, turtleback shape of the complex and at many, large 100s of metres-scale corrugations on the exposed surface parallel to the spreading direction (Tucholke et al., 2001; Escartín & Canales, 2011). Those corrugations resemble large-scale mullions observed along detachment faults on land. Therefore OCCs are often called megamullions (Tucholke et al., 1998; Dick et al., 2008). OCCs are delimited up-dip by a breakaway, where the fault initially nucleated and down-dip by a termination which marks the boundary between the OCC and hanging wall (Figs. 3, 4; Tucholke et al., 2001; Escartín & Canales, 2011). OCCs occur most frequently at segment margins, especially at the inside corners of the ridge/transform fault intersections (Tucholke et al., 1997).

The general geophysical features of OCCs are a positive gravity anomaly (Cannat et al., 1995; Blackman et al., 2009), higher induced magnetisation (possibly caused by magnetite production during serpentinisation of peridotite), locally higher seismic velocities and higher seismicity in relation to the crust created on the conjugate plate (Blackman et al., 2009). A very important feature of OCCs is the asymmetry in the spacing of magnetic anomalies across the spreading axis, with a broader spread of magnetic zones on the ridge flank containing the OCC. This shows that OCCs form in the more rapidly accreting plates of asymmetric spreading segments (Dick et al., 1991; Hosford et al., 2003, Baines et al., 2007; Escartín et al., 2008; Blackman et al., 2009; Mallows & Searle, 2012).

The generation of OCCs is related to the spreading rate (see Section 5). Most occur at slow-spreading ridges (full rate 20–55 mm/year; Dick et al., 2003) and, in second place, at ridges with a spreading rate of 12–20 mm/year (transitional between slow- and ultraslow-spreading ridges; Dick et al., 2003). However, the style of formation is controlled more by melt supply than by spreading rate. For example, the common presence of mantle rock at the OCC surface is related to a regime with limited magma supply, where the flux of magma is too low to generate continuous gabbroic plutons. Hence, we distinguish various types of OCC.

The first one is typical of magma-rich conditions (Dick, 2010). The structure of the crust is similar to
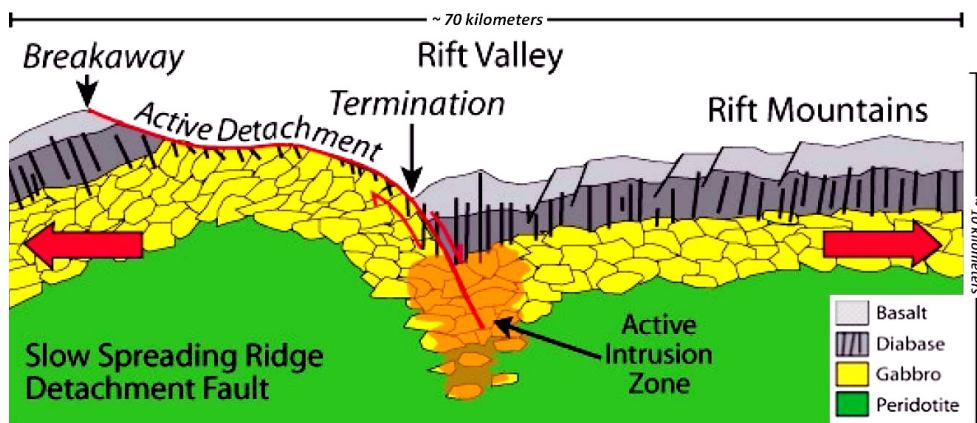
Fig. 3. Style of faulting at slow-spreading ridges with relatively high magma flux. Detachment fault exhumes oceanic core complex with predominance of gabbroic rocks on the sea floor
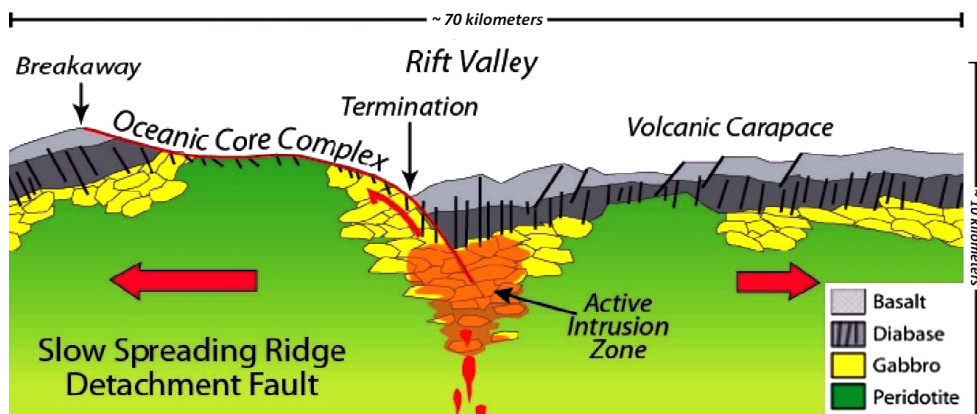

Fig. 4. Style of faulting at slow-spreading ridges with intermediate magma flux. Detachment fault exhumes oceanic core complex with relatively high amount of mantle rocks on the sea floor
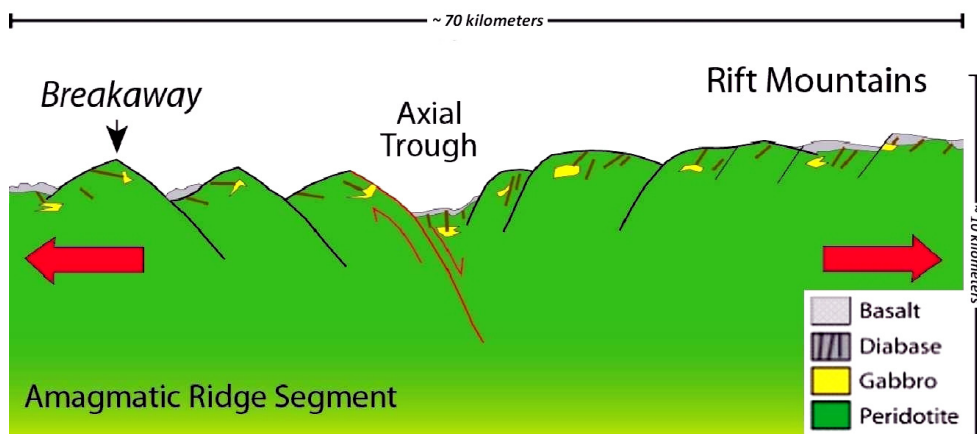

Fig. 5. Style of faulting at slow-spreading ridges with low magma flux. Block faulting exhumes peridotites with a minor amount of gabbroic rocks on the sea floor.

the model proposed by Dick (1989), which means it attenuates far from the segment centre. Gabbros are the commonest rocks observed on the OCC surface of this type (Fig. 3). The most important examples of such complexes are the Atlantis Massif at the Mid-Atlantic Ridge (MAR) and Atlantis Bank at SWIR (Dick, 2010).

The second type of OCC is related to sections of slow-spreading ridges with intermediate magma flux. Here, the structure of the crust can be best described with the Cannat (1996) model (Fig. 1B). Gabbros, as well as peridotites, are exposed at the surface (Fig. 4), reflecting the waning and waxing periods of magmatic activity. The best example
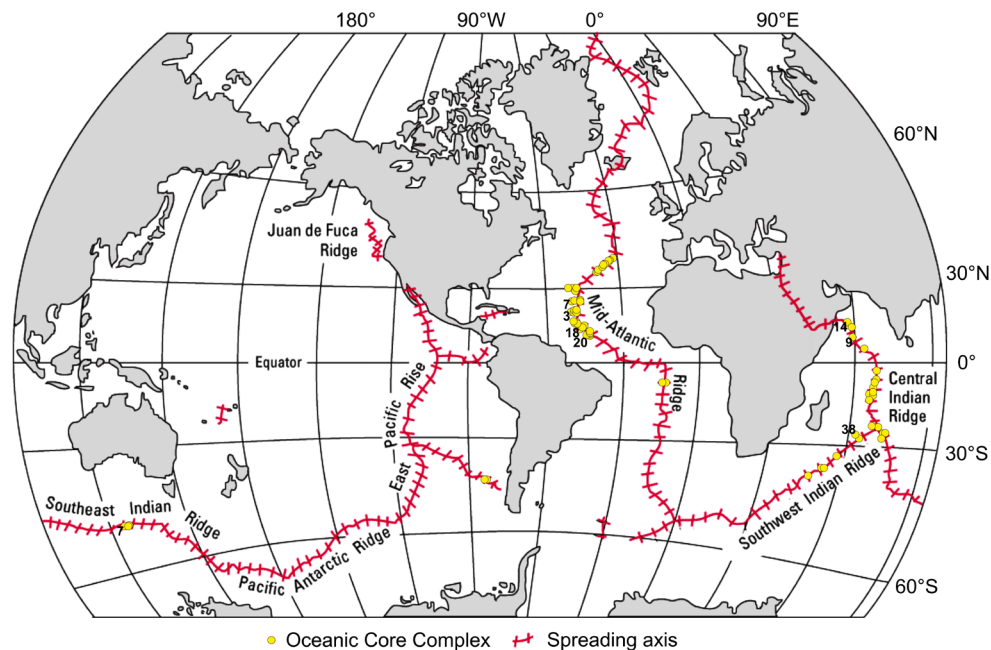
Fig. 6. Global distribution of oceanic core complexes associated with mid-ocean ridges. If more than one OCC was discovered at a given locality, the number of OCCs there is shown in black

of such an OCC is the Kane Megamullion at the Mid-Atlantic Ridge Kane (MARK) area (23°N; Dick, 2010).

When the magma flux is very low, peridotites and scattered basalts, with little or no gabbro appear at the sea floor (Fig. 5). The sea floor is 'smooth' compared to symmetric or asymmetric spreading (Cannat et al., 2006; Whitney et al., 2013), although still much rougher than at fast-spreading ridges, and block faulting is commoner than detachment faults with OCCs (Dick et al., 2003). This type of crustal structure is typical of ultraslow-spreading ridges (full rate < 12 mm/year) with the most pronounced examples found between 9 and 16°E along the Southwest Indian Ridge (SWIR) and in some sections along the Gakkel Ridge (Dick et al., 2003). Its formation is related to the Hess model as modified by Dick et al. (2003; see Fig. 1D).

5. Global distribution of OCCs

The importance of OCCs in crustal accretion is probably much greater than previously believed. Escartín et al. (2008) evaluated the 2,500 km section of the MAR between 12° and 35°N in terms of the symmetry of the spreading structure. Their research revealed an asymmetric accretion along almost half of this portion of the ridge. Baines et al. (2007) examined the eastern section of SWIR (54.75–62°E) in a similar way, and concluded that the individual segments in this section of SWIR spread asymmetrically. These studies trigerred a conclusion that OCCs constitute up to 25% of the crust along slow-spreading ridges (Smith et al., 2012). Here, we present a map of OCCs identified to date (Fig. 6). According to our literature analysis at least 172 OCCs have been discovered along mid-ocean ridges so far. This number does not include OCCs located far away from the active ridges, such as those identified near the Canary basin (Ranero & Reston, 1999; Reston et al., 2004), developed at back-arc basins (e.g., Godzilla Megamullion; Ohara et al., 2001, 2003a) or obducted on the continents as a part of an ophiolite (Nicolas et al., 1999; Nuriel et al., 2009; Tremblay et al., 2009; Manatschal et al., 2011; Maffione et al., 2013; Jousselin et al., 2013; Lagabrielle et al., 2015). Almost half (81) of the OCCs discovered are located at the MAR, with a high disparity in the frequency of occurrence between the northern (79) and southern (2) parts. Most of the others are situated along the other slow-spreading ridges: SWIR (43) and the Central Indian Ridge (35). Only 13 OCCs occur at intermediate spreading ridges: the Southeast Indian Ridge (SEIR; 11) and the Chile Ridge (2). No OCC has yet been found along fast-spreading ridges.

The full list of OCCs, together with spreading rate, is given in Table 1. Two OCCs at 5°05′S are located at the inside and outside corners of the ridge and a transform fault. They originally formed together as one OCC and then split about 0.5 Ma ago (Reston et al., 2002; Planert et al., 2010). The 15°45′N OCC is adjacent to the MAR on the western side and

Table 1. List of Oceanic Core Complexes (OCCs) according to their geographical location. MAR – Mid-Atlantic Ridge, SEIR – Southeast Indian Ridge, SWIR – Southwest Indian Ridge, spl – spinel, ol – olivine, opx – orthopyroxene, cpx – clinopyroxene, pl – plagioclase, PBP – plagioclase-bearing peridotites, SP – spinel peridotites, Cr# – chromium number (the molar Cr/(Al+Cr) ratio), Mg# – magnesium number (the molar Mg/(Mg + Fe) ratio), HF – hydrothermal field. The OCCs, in which peridotites were sampled, are shown in bold. Where serpentinites occur, they were included into the group of peridotites. See Section 6 for a discussion of their origin. Troctolites are included into gabbros. Spreading rates taken either from references specified or from Yu et al. (2013).

Locality	Number of OCC's	Full spreading rate (mm/year)	Main references	General sample description (% = wt.%)	Description of peridotites	Mineral chemistry of peridotites
5°05'S (IC High), MAR	1	32	Reston et al. (2002); Planert et al. (2010)	Mostly gabbros, some peridotites	Serpentinized strongly mylonitized; only fault gouge	No data
5°05'S (OC High), MAR	1	32	Reston et al. (2002)	Not sampled	–	–
13°02'N, MAR	1	24	McLeod et al. (2009); Wilson (2010); Kostitsyn et al. (2012)	Mostly gabbros, diabases and basalts, 2% of peridotites; Ashadze I & Ashadze II HF's	Serpentinized peridotites	No data
13°19'N, MAR	1	24	McLeod et al. (2009); Wilson (2010)	Mostly basalts, many peridotites (~22%), few gabbros (<2%); active HF	Protogranular massive peridotites subsequently mylonitized; serpentinite schist of the fault gouge	No data
13°30'N, MAR	1	24	Beltenev et al. (2007); McLeod et al. (2009); Wilson (2010)	Mostly basalts, many peridotites, few gabbros (~2–3%); Semyenov HF	Serpentinized peridotites	No data
13°48'N, MAR	1	24	McLeod et al. (2009)	Mostly basalts, many peridotites (~22%)	No data	–
Other between 12°40' to 13°45'N, Segment 13°, MAR	20	24	Smith et al. (2006); Smith et al. (2008)	Not sampled	–	–
Logatchev Massif	1	24	Schroeder et al. (2007); Grevemeyer et al. (2013); Shipboard scientific party (2003)	Mostly peridotites (~70%) and gabbros; active HF	Plastically deformed harzburgites; serpentinized	No data relevant for this paper
14°54'N, MAR	1	24	Fujiwara et al. (2003)	Only peridotites	No data	–
Other between 14°20' and 15°20', Segment 15°, MAR	18	24	Smith et al. (2008)	Not sampled	–	–
15°40'N, MAR	1	25	Fujiwara et al. (2003)	Not sampled	–	–
15°45'N, MAR	1	25	Escartín et al. (2003)	Mostly gabbros, many diabases and peridotites	Serpentinized peridotites, not deformed; dunites impregnated and changed into troctolites	Cr# in spl indicates 14.3–15.3% of partial melting
16°20'N, MAR	1	26	Escartín & Cannat (1999)	Not sampled	–	–

Locality	Number of OCC's	Full spreading rate (mm/year)	Main references	General sample description (% = wt.%)	Description of peridotites	Mineral chemistry of peridotites
South Core Complex at 16°25'N, MAR	1	26	Smith et al. (2014)	Mostly basalt and diabase, many peridotites (~23%), some gabbro (~8%)	Serpentinized peridotites	No data
22°19'N, 10 km west off-axis, MAR	1	25	Dannovski et al. (2010)	Mostly peridotites (~55%), many diabases	100% serpentinized harzburgites with relics of plastic mantle flow; ol, opx, probably cpx, no plag	No data
West of the 22°19'N OCC, MAR	1	25	Dannovski et al. (2010)	Not sampled	–	–
23°16'N, 46°31'W; 22°01'N, 45°48'W & 21°18'N, 45°39'W, MAR	3	25	Tucholke et al. (1998)	Not sampled	–	–
Kane Megamullion at 23°30'N, MAR	1	29	Dick et al. (2008); Dick et al. (2010); Tucholke et al. (2013)	Mostly peridotites (~42%), many gabbros and basalts; active HF	Many harzburgites with relics of plastic mantle flow; 13.6% plagioclase peridotites with <1% of plag mostly	Cr# in spl indicates 11.3–13.8% of partial melting; 0.78–0.82 Mg# in ol within PBP; 0.89–0.92 Mg# in cpx in PBP vs 0.91–0.94 in SP
West of the Kane Megamullion, MAR	1	29	Tucholke et al. (1998)	Not sampled	–	–
TAG at 26°08'N, MAR	1	21	Zonenshain et al. (1989)	Mostly diabases and gabbros, no peridotites; TAG HF	–	–
26°17'E, 46°25'W, MAR	1	21	Tucholke et al. (1997)	Mostly basalt, some peridotites (~17%)	serpentinized	No data
Dante's Domes at 26°35'N, MAR	1	18	Tucholke et al. (2001)	Mostly basalt, much diabase, some peridotites	Serpentinites, higly altered	No data
Other between 25°34 and 26°58'N, MAR	7	18	Tucholke et al. (1998)	Not sampled	–	–
Atlantis Massif at 30°08'N, MAR	1	24	Karson et al. (2006); Tamura et al. (2008); Blackman et al. (1998); Blackman et al. (2002a); Schroeder & John (2004); McCaig (2010)	70% Peridotites/30% Gabbro; Lost City HF	Fault gouge assemblage and massive peridotites, half of them plag-bearing with 0.8–13% of plag	Cr# in spl indicates 15.0–18.3% of partial melting; 0.85–0.90; 0.85–0.91 Mg# in ol within PBP vs 0.90–0.9 in SP; 0.88–0.92 Mg# in cpx in PBP vs 0.90–0.93 in SP
The southern OCC at 29°56'N, MAR	1	24	Cann et al. (1997)	Many peridotites and basalts	Serpentinites of fault gouge assemblage	No data
The western OCC at 30°17'N, 9 km west off-axis, MAR	1	24	Blackman et al. (2002b); Blackman et al. (2008); Baines et al. (2003)	Not sampled	–	–

Locality	Number of OCC's	Full spreading rate (mm/year)	Main references	General sample description (% = wt.%)	Description of peridotites	Mineral chemistry of peridotites
Keystone Block between the western OCC and Atlantis Massif, MAR	1	24	Blackman et al. (2008)	Not sampled	-	-
Rainbow Massif, 36°14'N, north of AMAR segment, MAR	1	22	Andreani et al. (2014); Fouquet et al. (1998); Ildefonse et al. (2007); Gente et al. (2008); Dyment et al. (2009)	Mostly peridotites (~50%) and sediments, some basalts, hydrothermal products and gabbros (up to ~4%), diabase Rainbow, Ghost City and Clamstone HF's	Harzburgites equilibrated with spinels, serpentinized to varying degrees; some dunites	No data
Saldanha Massif at 36°30'N, MAR	1	25	Gràcia et al. (2000); Miranda et al. (2002)	Mostly peridotites and basalts; Saldanha HF	Only serpentinites	No data
Other between 33°30' to 38°30'N	8	23	Gràcia et al. (2000)	4 sampled, **3 with peridotites** and minor gabbros, 1 only with dolerites, HF in 2 of them	Serpentinites (1 site) and serpentinized harzburgites (2 sites)	No data relevant for this paper
Dragon Flag OCC at 49°39'E, SWIR	1	14	Zhao et al. (2013)	Mostly basalts, some peridotites, Dragon Flag HF	Serpentinized	-
53°E, SWIR	2	15	Zhou & Dick (2013)	**Mostly peridotites, many diabases, few gabbros in the western OCC**; Only gabbros in the eastern OCC	Serpentinized harzburgites, granular and mylonitic texture	Cr# in spl indicates 12% of partial melting
Atlantis Bank at 57°23'E, SWIR	1	14	Dick et al. (2000); Baines et al. (2003); Zhou & Dick (2013)	Mostly gabbros, many peridotites (up to 28%)	Partially serpentinized with protogranular and porphyroclastic texture	No data
FUJI dome at 63°45'E, SWIR	1	14	Fujimoto et al. (1999); Searle et al. 2003	3 Gabbros, 1 peridotite	Serpentinized Harzburgite	No data
Other between 61.2° and 65.5°E, SWIR	38	14 (30 ancient)	Cannat et al. 2009	Not sampled	-	-
25°S, Central Indian Ridge	1	64	Mitchell et al. (1998); Sato et al. (2009); Morishita et al. (2009)	Mostly basalts, many gabbros, few peridotites (~8%)	Fault gouge and massive peridotites. The latter are 2 cpx-harzburgites; one of them is plagioclase-bearing	Cr# in spl indicates 13–15% of partial melting; Mg# in ol and opx are similar for SP and PBP (~0.91)
Uraniva Hills at 25°18'S, Central Indian Ridge	1	64	Kumagai et al. (2008); Nakamura et al. (2009)	Mostly gabbros, few peridotites (~4%)	Plagioclase dunite, coming from the lower crust	Mg# in ol ~0.92; ~0.3 Ni wt.% in ol
m3 at 9°35'S, Central Indian Ridge	1	26	Kamesh Raju et al. (2012)	Only basalts	-	-

Locality	Number of OCC's	Full spreading rate (mm/year)	Main references	General sample description (% = wt.%)	Description of peridotites	Mineral chemistry of peridotites
Other between 8° and 17° S, Central Indian Ridge	5	46	Yi et al. (2014)	Mostly peridotites (4 of 5 sites; ~39%), many basalts and diabases, some gabbros (~11%)	Serpentinized harzburgites, some with coarse-grained granular texture; ol, opx, spl, cpx present	No data
m2 at 7°00'S, Central Indian Ridge	1	32	Kamesh Raju et al. (2012)	Only basalts	-	-
Vityaz Megamullion at 5°30'S, Central Indian Ridge	1	31	Drolia & DeMets (2005); Kamesh Raju et al. (2012)	Mostly basalts and peridotites (~50%)	Serpentinized	No data
5°6'N, Central Indian Ridge	1	25	Yu et al. (2013)	Not sampled	-	-
8.8–10.4°N, Carlsberg Ridge - Central Indian Ridge	9	25	Han et al. (2012)	Not sampled	-	-
Varun Bank at 13°22'E, 59°22'N, NW of the Owen fracture zone, Central Indian Ridge, off axis	1	120 (ancient)	Mudholkar et al. (2012)	Mostly peridotites and gabbros	No data	-
12.3–15.6°N, Sheba Ridge, Central Indian Ridge	14	40	Chamot-Rooke et al. (2008)	Not sampled	-	-
26°05'S, 70°30'E; 26°00'S, 70°40'E & 27°28'S, 73°12'E, SEIR	3	56	Bartsch (2014)	Not sampled	-	-
124°10'–125°20'E, sub-segment B3E, AAT, SEIR	7	88	Okino et al. (2004)	Not sampled	-	-
125°45'E, Segment B4, AAT, SEIR	1	88	Christie et al. (1998)	Only basalts	No peridotites	-
84°30'W, Segment V6, Chile Ridge	1	53	Karsten et al. (1999); Tebbens et al. (1997)	Not sampled	-	-
84°50'W, Segment V6, Chile Ridge	1	53	Karsten et al. (1999); Tebbens et al. (1997)	Not sampled	-	-

located to the north of the Fifteen-Twenty fracture zone (Escartín & Cannat, 1999; MacLeod et al., 2002; Escartín et al., 2003; Fujiwara et al., 2003; MacLeod et al., 2011). The 16°20′N detachment fault has never been sampled. However, peridotites were found in the proximity suggesting it may be an OCC (Escartín & Cannat, 1999). The TAG OCC (Tivey et al., 2003; Canales et al., 2007; de Martin et al., 2007; Zhao et al., 2012) is the only one where gabbros make up 100% of the sampled material from the plutonic footwall (Zonenshain et al., 1989; Reves-Sohn & Humphris, 2004). The only serpentinic minerals are embedded in grey-blue clay (Zonenshain et al., 1989). Keyston Block represents a detachment fault, where an OCC has not fully developed yet. The lower crust and the mantle rocks have not yet been unroofed (Cann et al., 1997; Blackman et al., 2008). The western OCC at 30°17′N has not been sampled so far (Blackman et al., 2008), but some corrugation-like structures have been identified on its surface (Blackman et al., 2002b).

Two potential OCCs in the segment 53°E have been identified based on domal shape, corrugations and plutonic rocks found on their surface (Zhou & Dick, 2013). At the eastern OCC, a 250-kg-block of gabbro was taken by TV grab, whereas peridotite predominates in the western OCC. In Atlantis Bank, no past hydrothermal activity has been discovered so far. However, evidence of that could have been removed during erosion, as Atlantis Bank was once an ocean island (Palmiotto et al., 2013). Although Atlantis Bank is the only OCC discovered so far in the region, asymmetric spreading in individual segments between 54.75 and 62°E (Baines et al., 2007) suggests that more OCCs may exist in the proximity. Thirty-eight corrugated surfaces located between 61.2° and 65.5°E and the 30-Ma chronozones identified by Cannat et al. (2009) are related to detachment faulting and potentially OCCs. The total surface of these OCCs constitutes about 4% surface of the area analysed (Cannat et al., 2006). Some of the OCCs located between 63.5 and 64.5°N were also described by Searle & Bralee (2007). Interestingly, the OCCs are more frequent beyond the chronozones older than 10 Ma (Cannat et al., 2009), when full spreading rate was higher (30 mm/year) compared to the present rate. This might suggest that detachment faulting was relatively commoner between 10 and 30 Ma, whereas amagmatic accretion with block faulting, typical of ultraslow spreading, became dominant after 10 Ma.

Among nine OCCs in the northern portion of the Central Indian Ridge –the Carlsberg Ridge between 8.8–10.4 °N, six are located near the rift valley and three are off-axis. Fourteen OCCs located fur-

ther northeast, northeast of the Sheba Ridge have mainly been identified by their geomorphological features (Chamot-Rooke et al., 2008; Fournier et al., 2008, 2010). Interestingly, there is an asymmetry of the spreading and the crustal thickness in the Gulf of Aden with the thinner crust also in the plate northeast of the Sheba Ridge (d'Acremont et al., 2006). The Varun Bank is situated northwest of the Owen fracture zone at 13°22′ embedded in the 52-Ma-old crust (Exon et al., 2011). The full spreading rate during the generation of the OCC was 120 mm/year (Exon et al., 2011), which would be the fastest spreading rate estimated for OCCs all over the world.

The three OCCs at the westernmost SEIR have recently been discovered based on sea floor bathymetry by the German INDEX expeditions (Bartsch, 2014). The OCCs along the Antarctic-Australian Discordance (AAT) have been identified as OCCs based on prominent corrugations (up to 55 km; Okino et al., 2004) and gravimetric data predicting peridotites in the footwall (Christie et al., 1998). Only basalts were found over segment B4 (see Table 1; Pyle et al., 1992; Palmer et al., 1993; Pyle, 1993; Christie et al., 1998). No sampling occurred in subsegment B3E (Table 1; Okino et al., 2004). Two groups of megamullions resembling OCCs found along the Chile Ridge (segment V5) have not been sampled so far. However, serpentinites and fresh peridotites were recovered in the adjacent segment V5 (Karsten et al., 1999).

6. Peridotites recovered from OCCs

Based on geophysical studies, ultramafic rocks are often assumed to occur at the surface or subsurface of OCCs on account of their geophysical features (Christie et al., 1998; Okino et al., 2004). Among the 172 OCCs listed above, only ~39 were sampled by submersible, dredge or drilling (Table 1). Among these, peridotites were absent in seven OCCs. At least four of the seven were not sampled extensively enough to exclude the presence of peridotites; only basalts were found. Among 32 OCCs where mantle rocks were sampled, 20 are located along the MAR, 4 along the SWIR, and 8 along the Central Indian Ridge (Table 1).

6.1. Mid-Atlantic Ridge

With the exception of Atlantis Bank on the SWIR, the best-known OCCs, including the most extensively sampled 15°45′, Kane Megamullion and

Atlantis Massif OCCs, are located along the MAR. Oceanic expeditions have recovered mantle rocks from 20 OCCs along the ridge, mostly between the Marathon Fracture Zone (12°30′N) and the Azores Islands (38°N).

The only OCC peridotite samples from the southern MAR come from the western (inside-corner) 5°05´S OCC. Three dredges over the OCC recovered mostly gabbro. Some peridotites were found in the upper part of the footwall. They are strongly sheared and mylonitised. They likely constitute detachment fault gouge (Reston et al., 2002).

MacLeod et al. (2009) sampled 4 of the 24 OCCs from Segment 13°. The 13°19′N OCC consists of two structurally different parts. The western portion is rugged, more elevated, and exposes mainly basalt (only 11% peridotites). The eastern portion is enclosed in a smooth dome and exposes serpentinised peridotites (41%). The 13°30′N OCC has a similar structure and composition (MacLeod et al., 2009). Mostly basalts and peridotites have been collected along the OCC (Beltenev et al., 2007; MacLeod et al, 2009). Also in the 13°48′N OCC, most of the peridotites were recovered from a smooth domal surface, constituting 20% of the dredges. Additionally, MacLeod et al. (2009) provided some supplementary data on the OCC located further south, between 12°55′ and 13°12′N. The sole dredge over this OCC contained 2% (0.34 kg) peridotites (MacLeod et al., 2009; Wilson, 2010). Generally, it is difficult to infer the origin of peridotites from these data. However, the textures of the peridotites from the 13°19′N OCC indicate that they make up the footwall and are not only fault gouge (Table 1).

No information is available on peridotite dredged over the 14°54′N OCC (Fujiwara et al., 2003). Three of four boreholes from site 1270 at the Logatchev Massif yielded almost exclusively peridotites. Many gabbroic veins cutting the peridotites suggest the holes are in the vicinity of a larger gabbro body (Shipboard Scientific Party, 2003; Schroeder et al., 2007). Two boreholes (1275B, D) drilled in the OCC located on the opposite inside-corner, north of the Fifteen-Twenty fracture zone, recovered mostly gabbro and some troctolite (Schroeder et al., 2007). The troctolites appear to be impregnated dunites of mantle origin (Shipboard Scientific Party, 2003). More peridotites (~20%) were drilled and dredged on the 15°45′N OCC (Escartín et al., 2003). About 40–45% of them come from the detachment surface, the rest from the footwall. These are serpentinised but revealed no trace of high-temperature deformation. Additionally, we have estimated the degree of partial melting based on the molar Cr/(Al+Cr) ratios (Cr#) in six spinel grains (0.38–0.42; Escartín et

al., 2003) using the model of Hellebrand et al. (2001). Our results indicate that the peridotites underwent 14.3 to 15.3% partial melting. Finally, serpentinised peridotites have recently been found by Smith et al. (2014) at South Core Complex at 16°25′N. They appeared in three of six dredges in the area constituting ~23% of the hauls, with ~8% gabbro.

Heavily serpentinised harzburgites predominate in 7 of 13 sampling sites on the southern wall of the 22°19′N OCC. They show relics of high-temperature crystal-plastic deformation, but no lower temperature deformation. Diabase and basalt predominate on the conjugate site of the rift (Dannovski et al., 2010). The best-studied and sampled OCC in terms of peridotite exposures is the Kane Megamullion. The core complex consists of six opposing domes, constituting a southern, central and northern region. About 1,238 kg of peridotites were collected by dredges and ROV dives, making up 42 wt.% of all rocks recovered, and being the most abundant (63 wt.%) in the central region. In the southern part, dunites constituted about half of all peridotites, contrasting to only 1–2% in the central and northern regions. Roughly 75–80% of peridotites were sampled from the detachment surface with their typical mineral phases and lower temperature deformation. The rest of the mantle rocks came from the headwalls and fault scarps that cut down into the OCC footwall. Some exhibit crystal-plastic deformation characteristic of fault surfaces that rooted into crystalline peridotite at high temperatures (Dick et al., 2008). Most of the peridotites are spinel harzburgites (62%). However, plagioclase-bearing peridotites are relatively common (14%), mostly from Adam & Eve domes. They usually contain less than 1% of relict plagioclase and its alteration products (Dick et al., 2010). Dick et al. (2010) used spinel Cr#s to estimate the degree of partial melting with the model of Hellebrand et al. (2001). They found a range 11.3–13.8% of partial melting, with the lowest values near the transform fault.

Five dives were performed in the southern hill of the Dante's domes OCC recovering two serpentinites from the bottom sections. Both were highly altered and subsequently veined by chlorite and amphibole. No primary phases or structures were present (Tucholke et al., 2001). At the 26°17′N OCC, situated in the vicinity, peridotites were found in one of six dredges. Basalt was recovered in the others. The peridotites are serpentinised, but they probably come from the plutonic footwall (Tucholke et al., 1997).

Dives to the southern wall of the Atlantis Massif OCC recovered 70% peridotites with 30% gabbros

and gabbro veins. These peridotites are variably altered (mainly serpentinised) rocks with a harzburgitic protolith. The peridotites have a porphyroclastic texture representing moderately distributed high-temperature crystal-plastic deformation (Karson et al., 2006). The central part of the OCC north of the transform wall was drilled by IODP, penetrating to 1,415 m in massive gabbro (Shipboard Scientific Party, 2005a, b). Few serpentinised peridotites are present in the upper 100 m of Hole 1309B and 1,415m deep Hole 1309D (0.5–3%) and in the following 400 m section of 1309D (4%; Shipboard Scientific Party, 2005a). No peridotites were recovered from the lower section of the latter hole (Shipboard Scientific Party, 2005b). Nevertheless, several olivine-rich troctolite intervals are interpreted as mantle peridotite hybridised by progressive reaction with basaltic melt (Drouin et al., 2007, 2009, 2010; Suhr et al., 2008). The peridotites from Hole D and from the upper sections of Hole B appear to be residual mantle harzburgites. Those from Hole D were subsequently impregnated by basaltic melt and contain interstitial plagioclase, while those from Hole B are variously serpentinised protogranular harzburgites (Tamura et al., 2008). The authors suggested 15.0–18.3% degree of partial melting in the spinel stability field. Additionally, the southern OCC on the opposite side of the Atlantis fracture zone was sampled by Cann et al. (1997). They found serpentinised peridotites in two of five dredges: one on the summit and one on the sloping rift valley wall.

Mantle peridotites (spinel harzburgites and minor dunites) were the predominant rock type recovered from the footwall of the Rainbow Massif (36°14′N). Some of them show evidence of late melt-rock (e.g., enhanced REE concentrations) and fluid-rock (e.g., enhanced Li and U concentrations) interaction. They are variously serpentinised, and some are talc-serpentine schists typical of fault gouge, found where detachment faulting cuts mantle peridotite. However, some show no deformation and are likely a part of the footwall block. Minor gabbros and gabbroic veins were also recovered (Ildefonse et al., 2007; Andreani et al., 2010, 2014). Serpentinites were found in four of five dives over the Saldanha Massif at 36°30′N, being dominant in some of them. Fractured basalt rubble recovered in the dredges is interpreted as hanging wall debris rafted on the detachment fault surface. Thus, the basement below the fault surface is largely serpentinised peridotite (Miranda et al., 2002).

Of the eight other potential OCCs from the region (Gràcia et al., 2000), four have been sampled (ARCYANA, 1975; Gràcia et al., 1997; Ribeiro da Costa et al., 2008). Three of the OCCs sampled contain serpentinised peridotites (Gràcia et al., 1997; Ribeiro da Costa et al., 2008). The two most southerly OCCs have been described by Gràcia et al. (1997). Peridotites, mostly serpentinised harzburgites, make up ~45 and ~85 wt.% of the dredged material, respectively. They usually predominate at the central part of these massifs, whereas equally abundant diabases make up the lower slopes. The diabases likely cross-cut the peridotites. Additionally, microgabbros occur, but very rarely. It is not clear whether peridotites predominate in the footwalls or just at the surface of the detachment faults. Hydrothermal fields were found in two of the four sampled OCCs (Gràcia et al., 2000; Escartín et al. 2014).

6.2. Southwest Indian Ridge

Partially serpentinised peridotites in the OCCs along the SWIR were reported over the Dragon Flag OCC, FUJI dome, Atlantis Bank and the western 53°E OCC. Although two dredges from the Dragon Flag OCC during Edul cruise (Mével et al., 1997) found only basalts, a plutonic footwall was expected based on bathymetry and seismic surveys, and gabbro was proposed (Zhao et al., 2013). However, this interpretation cannot be unique, as density, and P-wave and S-wave seismic velocities for gabbros and partially serpentinised peridotite overlap each other (Miller & Christensen, 1997). In fact, some serpentinised peridotites have been sampled very recently by another Chinese group (Zhou, 2015). More sampling occurred over the Fuji dome, but only one, intensely sheared, serpentinised harzburgite was sampled by submersible from the middle part of the northern slope of the dome. Being 1 of 47 samples collected in three dives, it constitutes 2.1% of the material recovered. More gabbroic rocks were recovered (two gabbros and one troctolite). These rocks imply outcrops of the lower crust and the upper mantle (Searle et al., 2003).

The Atlantis Bank OCC was drilled to 1,508 m on a wave-cut platform at the centre of the palaeo-ridge segment at which it formed. Other than two dykes in the upper few hundred metres, only gabbro was cored (Dick et al., 2000). Forty dredges recovered 1,230 kg of rock, of which 47% was gabbro and gabbro mylonites and 28% partially serpentinised peridotite and talc-serpentine schist. Low on the transform wall, granular peridotites were recovered in abundance, while sheared serpentinites and talc-serpentine schists were found overlying massive gabbro mylonites higher on the wall. The latter are interpreted as representing a discontinu-

ous sheet of fault gouge that lubricated the detachment fault by intrusion along it from where it cut uplifted mantle rock in the vicinity of the transform. The distribution of rock types recovered in dredges and by submersible shows that there is a contact between lower crustal gabbros and massive mantle peridotite that runs for nearly 30 kilometres along the eastern transform wall, progressively shoaling with increasing age to the south.

Ultramafic rocks have been found in four dredges performed over the western OCC at the segment 53°E (Zhou & Dick, 2013). Two dredges (550 kg) contained only peridotites with minor breccia. Two hundred fifty kg of material from another dredge contained mostly peridotites with minor diabase. Diabases predominate in the fourth dredge (17 kg), although gabbroic rocks and peridotites are also present. Zhou & Dick (2013) suggested that the dredged peridotites underwent 12% of partial melting based on Cr# in spinels.

6.3. Central Indian Ridge

Peridotite exposures along the Central Indian Ridge are reported from the Varun Bank, the Vityaz Megamullion and the 25°S OCC, as well as from several newly discovered OCCs between 8 and 17°S. No data are available for the Varun Bank peridotites at this time. Two peridotites were collected from the Vityaz Megamullion. One from the southeastern part of the megamullion adjacent to the Vityaz fracture zone was described by Kamesh Raju et al. (2012) as serpentinised peridotite. Peridotites have been found in four of the five OCCs identified between 8 and 17°S (8°10', 9°55', 10°50',11°20' and 13°15'S). These serpentinised harzburgites made up from 37 to 60% of the recovered material in these OCCs. Constituting from 66 to 80% of the plutonic material, they were more abundant than gabbros. Some peridotites show coarse-grained granular textures, whereas evidence of crystal-plastic deformation is rare. Gabbroic veins have not been observed within the mantle rocks.

Two types of peridotites were recovered by dives on the 25°S OCC (Morishita et al., 2009). The first type is highly deformed serpentinised peridotite fault gouge associated with the detachment surface. The second type is massive granular peridotite. Two of these were sampled from the top of the dome's west slope adjacent to the rift valley. They constitute roughly 8% of the material recovered from the largely gabbroic megamullion. Both samples are diopside-bearing harzburgites. They underwent 13–15% partial melting, as Morishita et

al. (2009) calculated from the spinel Cr#s. One sample was altered due to reaction with granitic veins. Interstitial plagioclase is present (Morishita et al., 2009). A plagioclase dunite recovered from the Uraniva Hills, located further east (70°10'E) along the spreading direction, probably derives from the lower crust rather than from the mantle as its Ni content is relatively low (Nakamura et al., 2009; Table 1).

7. Discussion

7.1. Mantle peridotites and associated basalt

The percentage of peridotites in samples recovered from OCCs varies widely. OCCs with no occurrence of peridotites as well as those predominated by mantle rocks are listed above (Table 1). These data should be interpreted with caution, especially in the case where few plutonic rocks were found. The amount of plutonic rocks in the footwall is generally higher than that estimated from dredges, as basalts and diabases constitute a significant part of the haul. Whereas the peridotites, gabbros and some diabases underwent greenschist facies or higher-temperature alteration, the basalts are generally weathered, but otherwise unaltered, containing fresh plagioclase and olivine phenocrysts. This demonstrates a very different origin and these are best interpreted as hanging wall debris or even products of off-axis volcanism, as may have occurred at the Kane Megamullion (Dick et al., 2008). Diabases are more indeterminate as they could have come from either the hanging wall or the footwall where they may represent inliers of the dyke-gabbro transition in the footwall, or as fragments of the extrusive-dike transition in the overlying hanging wall (e.g., Dick et al., 2008; MacLeod et al., 2009; Wilson, 2010).

7.2. Percentage of peridotites in the footwall

Although minor inliers of the dyke-gabbro have been found in two (Atlantis Bank; Dick et al., 2000; Kane Megamullion; Dick et al., 2008) of three best-sampled OCCs, the available data (see Table 1; Sections 7.1 and 7.4; Escartín & Canales, 2011) show that OCC detachment footwalls are composed largely of plutonic rocks. Therefore, we find it useful to examine the ratio of peridotites to gabbroic rocks. For this reason, we have compiled data on total weight (when provided) or number of peridotites
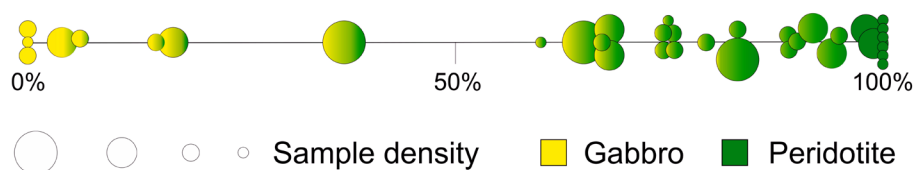
Fig. 7. The axis showing the percentage of peridotites among all plutonic rocks (peridotites + gabbroic rocks) for various OCCs. Peridotites predominate in most OCCs, as indicated also by the green colour. The empty circles show the degree of sampling. The largest circle (left) indicates very extensive sampling (725–1,908 kg). The smaller circles (right) correspond to moderately high sampling (40–68 kg or 24–73 samples), moderately low sampling (5.5–10 kg or 4–15 samples) and very low sampling (single sample or a general description), respectively. The western 53° OCC, with 817 kg of collected rocks, has been moved to the second group as the amounts of gabbro and peridotite within the dredges are not strictly constrained (see text). About 250 kg of plutonic rocks were collected in the eastern 53° OCC along the SWIR and the Rainbow Massif along the MAR. The former was classified in the moderately low-sampled group as one gabbroic block made up the haul. The latter was assigned to the moderately high-sampled group as only pie diagrams have been published to date (Andreani et al., 2014) which lowers the precision of our estimates

and gabbroic rocks in all OCCs sampled. Plutonic rocks were found in 35 of the 39 OCCs sampled. The percentage of peridotites varies from 0 to 100% (Fig. 7). Considering only the well-sampled OCCs (see caption to Fig. 7), the range is not significantly lower, being between 4 and 99%. The broad range we find shows that OCCs represent very different crustal architectures. We can identify at least five of them. At one extreme, crustal rocks are virtually absent (Fig. 1D), similar to those from the western 53° OCC (Zhou & Dick, 2013; Table 1). Three intermediate cases include 1) peridotites overlain by pillow lavas with relatively few associated dykes, as represented by the central domes of the Kane Megamullion (Dick et al., 2008), 2) plum-pudding of small gabbro bodies intruded into peridotite, overlain by dykes and pillow lavas, as to the north and south of the Fifteen-Twenty fracture zone (Cannat & Casey, 1995; see Fig. 1C), 3) small plutons capped by dykes and pillow lavas intruding laterally into massive peridotite, as at the Atlantis Massif (Blackman & Collins, 2010; Blackman et al., 2011; see Fig. 1B). At the other extreme, there are large plutons that extend virtually over the full length of a second-order ridge segment, as at Atlantis Bank. A full cover of sheeted dykes and pillow basalts occurs here, represented by inliers of the dyke-gabbro transition, and abundant pillow basalt in hanging wall debris (Fig. 1B).

Our compilation suggests that the majority of OCCs represent either the plum-pudding model (Fig. 1C) or nearly amagmatic spreading (Fig. 1D). We observe that 77% of all OCCs, and 73% of highly sampled OCCs, contain more peridotites than gabbro (Fig. 7). At 4 of 11 highly sampled OCCs, at least 90% of the plutonic rocks are peridotites (Fig.7). These observations imply that the model of Dick et al. (2003) for magmatic segments on at ultraslow-spreading ridges might even be applied

to some ridge segments at slow-spreading ridges. However, this has to be treated with caution. Firstly, strongly oblique segments, characteristic of such spreading on ultraslow-spreading ridges, have not been described at slow-spreading ridges. Secondly, the proportion of gabbroic rock might be higher than calculated from the distribution of lithologies in the dredges. Unless there are large cross-faults or land-slips that cut down into the detachment footwall, serpentinite and talc-serpentinite fault gouge intruded laterally along the active fault plane may mask an underlying gabbro body, as at the Kane Megamullion (Dick et al., 2008; Xu et al., 2009) and the 15°45′ OCC (Escartín et al., 2003). This is related to the common presence of mantle peridotite in detachment fault regions. Furthermore, although it is often assumed that detachment fault root shallowly in the crust (Section 7.4), probably in the gabbro-dike transition zone (Escartín et al., 2003), given the abundance of peridotite mylonites, and crystal-plastically deformed amphibolitic gabbro mylonites in many OCCs (e.g., Kane Megamullion; Dick et al., 2008; Atlantis Bank; Dick et al., 1991, 2000), it would seem evident that detachment fault roots more deeply, passing through the dyke-gabbro transition. In this case, a significant part of gabbros could be cut and moved away with the hanging wall. Last but not least, massive gabbros are notoriously hard to dredge, but this refers to slow- as well as ultraslow-spreading ridges.

7.3. The origin of peridotites (fault gouge *vs* inside of the footwall)

As discovered in some OCCs, peridotites are very common rocks at the surface of detachment faults. However, the proportion of peridotites appears to be smaller under the surface of the footwall

(Dick et al., 2001, 2008; Escartín et al., 2003). We observe such a peculiar distribution of peridotites, because some of them are associated only with the detachment fault, related to the fact that serpentinised peridotites may easily lubricate a fault, relieving stress along the fault zone. Such serpentinised peridotites may originate from where the detachment fault roots into massive peridotite, either vertically where the crust is thin, or laterally, as in mantle peridotite emplaced into a transform zone, and migrate as a fault gouge up or along the fault. They are usually highly deformed and often consist of 100% alteration phases (serpentine plus talc; Dick et al., 2001, 2008; Morishita et al., 2009). Due to the extreme alteration, these peridotites have very limited use for evaluation of igneous petrogenesis. The remaining peridotites, however, are largely massive protogranular and porphyroclastic peridotites similar to those exposed in large peridotite massifs such as Table Mountain in the Bay of Islands Complex in Newfoundland, or in the Josephine Peridotite in the US states of Oregon and Washington. Where these occur in abundance, multiple dredges show that they are exposed over large regions, constituting large massifs exposed by detachment or block faulting onto the sea floor. As our data compilation shows, at least 18 of 32 OCCs in which peridotites were sampled contain massive peridotites (Table 1). We expect that the massive peridotite will be documented, at least locally, in most of the other 16 OCCs in the future.

7.4. What do massive peridotites represent?

When the lower crust is present, it is believed that the detachment faults root in gabbroic crust and not in the mantle (Dick et al., 2000; Escartín et al., 2003; Zhou & Dick, 2013). This is the case for the majority of OCCs, since gabbro plutons and gabbroic veins in peridotites are common throughout them (e.g., Karson et al., 2006; Dick et al., 2008; Morishita et al., 2009; Sections 6 and 7.2). Elsewhere, peridotite mylonites, representing the high temperature (600°C plus; Jaroslow et al., 1996) detachment faults where they rooted into upwelling mantle. Although these have not been found at all peridotite massifs, such fault zones are likely very narrow and easily missed by relatively few scattered dredges. Due to a strong contrast in physical properties with the underlying partially serpentinised peridotite, they are also easily removed by mass wasting. For example, while not previously reported from 14° to 17°N on the Mid-Atlantic Ridge, they have recently been found in the central and northern regions of

the 16.5°N detachment fault system by Smith et al. (2014). Thus, the massive peridotite outcrops represent direct emplacement of crystalline peridotite onto the sea floor on faults that rooted up to several kilometres into the mantle beneath the spreading axis or adjacent transform.

The massive peridotites are sampled by drilling, dredging or diving in landslip headwalls or talus ramps, or along high-angle faults that crosscut the detachment fault surface. These scarps and faults, by simple geometry, expose only a few hundred metres depth below the detachment footwall, and thus we can assume that the peridotites represent only the few hundred upper metres of the mantle emplaced along the plate boundary.

7.5. What is the typical degree of partial melting of abyssal peridotites?

The degree of partial melting of peridotites is reflected in spinel composition (Hellebrand et al., 2001). We checked available publications for spinel analyses in massive peridotites, and found five data sets. Assuming that the mantle major element source composition is uniform (this is not always the case, as shown by Dick & Zhou, 2015), the degree of mantle partial melting calculated for these data vary within a range of 11.3–18.3% (Table 1). Melting under ridges is subadiabatic, driven by the difference between the adiabat and the solidus depression with decreasing depth. Therefore, the degree of melting increases during magma upwelling, reaching the highest value at the top of the melting column. In this light, the 11.3–18.3% partial melting range represents the highest degree of partial melting under the ridge where they were sampled.

Considering the decreasing degree of melting from the centre to the ends of segments (Niu & Batiza, 1994) and the fact that only spinels coming from locations far from the segment ends are included in the calculations mentioned above, we might interpret the value ~18% as being at the high end of melting along slow-spreading ridges. For comparison, Dick et al. (2010) suggested 8% partial melting for the Kane Transform and Wang et al. (2013) noted a similar value (~7.9%) for the Gallieni and Gazelle fracture zones, using the same method (Hellebrand et al., 2001). One example, where a higher degree of partial melting is observed at a segment end, is at the Vema Transform (11°N, MAR, full spreading rate 27.2 mm/year) where a successive section of peridotite, gabbro, dykes and overlying basalts occur along the transform wall (Auzende et al., 1989). The peridotites located between 9.5 and

6 Ma isochrones display a range of 9–13.5% partial melting in their upper part, up to 1 km from their boundary with gabbros. However, the degree of partial melting throughout the older intervals oscillated between 5 and 10% (Bonatti et al., 2003). This range in the degree of partial melting is also displayed by peridotites in the Owen fracture zone and the Romanche fracture zone (Choi et al., 2008).

7.6. Plagioclase-bearing peridotites as indicators of interaction with trapped melt

The OCC peridotites are typically spinel harzburgites (Section 6), which can be explained by the relatively high degree of partial melting in the OCC peridotites (Section 7.5). On the other hand, they are relatively rarely plagioclase bearing in comparison to the abyssal peridotites from the transform valleys, where 38% of all peridotites contain plagioclase (Dick, 1989). Plagioclase in abyssal peridotite is usually interpreted to have resulted from interaction with transient trapped melt (Dick 1989; Bonatti et al., 1992; Rampone et al., 1997). Additional evidence for such interaction is a relatively low olivine and pyroxene Mg# (Coogan, 2013). The relatively small amount of plagioclase-bearing peridotites among the OCC peridotites facilitates the investigation on partial melting in the mantle, as original Cr# in spinels can be preserved, whereas reaction with late impregnating melts generally elevates the Cr# as Al goes into the plagioclase (Dick et al., 2010). On the other hand, the percentage of plagioclase in the plagioclase-bearing peridotites allows us to estimate the amount of trapped melt. For example, assuming a normative percentage of plagioclase in MORB as high as 50–55% (Wilkinson, 1986), we can estimate that ~2% of plagioclase indicates ~4% of trapped melt.

Careful mineral mode estimation in the OCC peridotites has revealed that plagioclase-bearing peridotites occur in every OCC where the estimation was made (Table 1). This is the case for the Kane Megamullion (Dick et al., 2010), the Atlantis Massif (Tamura et al., 2008) and the 25°S OCC (Morishita et al., 2009). Only interstitial clinopyroxenes and no plagioclase are reported by Dannovski et al. (2010) for 22°19'N at the MAR. However, the samples were 100% altered. Thus, the presence of plagioclase cannot be excluded even there. Plagioclase only ever occurs in part of the peridotites. This is the case for the Atlantis Massif and 25°S OCC. The plagioclase-bearing peridotites make up ~14% of

the mantle rocks in the most representative set of data, which is the Kane Megamullion.

In most specimens from the Kane Megamullion, the Atlantis Massif and the 25°S OCC, plagioclase constitutes less than 1% of plagioclase-bearing peridotite, although only in several samples approaching more than 5%. The average olivine and clinopyroxene Mg# is significantly lower in plagioclase-bearing peridotites than in spinel peridotites in the Kane Megamullion and the Atlantis Massif, while it is similar in the 25°S OCC (Table 1). However, the plagioclase also occurs as an interstitial phase in the latter. To summarise, it seems that many abyssal peridotites interacted with a MORB-like melt. The irregular distribution of plagioclase (see also Section 6) indicates a non-uniform flow of melt.

As mentioned above, plagioclase-bearing peridotites occur more frequently in the transform peridotites than the peridotites originating from OCCs. In addition, they show higher modal amounts of plagioclase, because the average volume of plagioclase exceeds 2% in the most plagioclase-bearing transform peridotites (Dick, 1989). The highly variable plagioclase contents indicate that the flow of transient melt was also non uniform (Dick, 1989). However, the greater abundance of plagioclase and the frequency of plagioclase-bearing peridotites suggest a more intensive late-stage melt impregnation in the transform peridotites than in the peridotites originating from OCCs.

7.7. Peridotite-hosted hydrothermal fields

Analysis of the literature (Table 1) shows that active hydrothermal fields have been found at 12 of 39 sampled OCCs, which suggests these provide exceptionally favourable conditions for their generation. Tivey et al. (2003), McCaig et al. (2007) and Tucholke et al. (2013) recognised the important role of active detachment faults as main conduits for hydrothermal circulation. The root zone of such a circulation can be located up to 11 km below the sea floor (Silantiev et al., 2009a, b). Thus, hydrothermal fluids extensively react with ultramafic rocks during ascent, buffering vent fluid chemistry, as in the case of the Lost City hydrothermal field at the Atlantis Massif (Kelley et al., 2001). It influences the composition of the ore minerals generated to those fluids. For example, massive sulphides hosted in peridotites at the Logatchev Massif display a peculiar composition (Petersen et al., 2009). Other hydrothermal fields hosted in peridotites have to be investigated in order to determine whether or not

they generate a new class of ore deposit, different from basalt-hosted deposits.

8. Conclusions

1. Oceanic core complexes are common features in the oceanic crust architecture of slow-spreading ridges. At least 172 oceanic core complexes have been identified on the basis of bathymetry and geophysical data. Most were discovered during the last decade. They occasionally occur as isolated massifs, but it is usual for them to occur in groups of up to 39 OCCs in one extended segment. Thus, we can expect to discover dozens of new OCCs as more detailed mapping occurs along slow-spreading mid-ocean ridges. Undoubtedly, there are also many hidden beneath the sedimentary cover far from active rifts. Therefore, detachment faulting is a common and not an anomalous mode of crustal accretion at slow-spreading ridges.
2. Only 39 of 172 OCCs have been sampled so far. However, as 32 of them contain peridotites, they are clearly common in their footwall. Moreover, peridotites predominate in the plutonic footwall of the majority of them. The high number of OCCs and their relatively large dimensions compared to other settings of oceanic crust where peridotites are involved allow earth scientists to focus on sampling of a complete section of the upper mantle and lower crust by extensive dredging, diving and drilling in megamullion systems.
3. Massive OCC peridotites represent the very top of the melting column beneath ocean ridges. They are typically spinel harzburgite and show 11.3–18.3% partial melting, assuming a primitive upper mantle source composition, in the segment centres, generally representing the maximum degree of melting along a segment. The degree of melting is lower in the segment ends and presumably in the lower part of the melting column.
4. The OCC peridotites often contain plagioclase, which together with low pyroxene and olivine Mg#s generally indicates a late-stage impregnation with MORB-like melt. The pattern of the plagioclase distribution suggests a non-uniform flow of melt.
5. Based on the above, OCC peridotites away from segment ends and transforms can be treated as a new class of abyssal peridotites. These differ from the transform peridotites by higher degrees of partial melting and lower interactions with subsequent transient melts. At the same time, we are aware that not enough sampling and analysis have been performed on OCC peridotites, and this distinction requires further substantiation. Therefore, we wish to emphasise that OCC peridotite samples represent an opportunity, not yet fully exploited, to investigate partial melting, melt transport, ultramafic-hosted hydrothermal processes and both large- and local-scale mantle heterogeneity.

References

Andreani, M., Ildefonse, B., Delacour, A., Escartín, J., Godard, M. & Dyment, J., 2010. Tectonic Structure and Internal Composition of the Rainbow Massif, Mid-Atlantic Ridge 36°14′N. Abstract presented at *AGU Chapman Conference*, Agros, Cyprus.

Andreani, M., Escartín, J., Delacour, A., Ildefonse, B., Godard, M., Dyment, J., Fallick, A.E. & Fouquet, Y., 2014. Tectonic structure, lithology, and hydrothermal signature of the Rainbow massif (Mid-Atlantic Ridge 36°14′N). *Geochemistry, Geophysics, Geosystems* 15, 3543–3571.

ARCYANA, 1975. Transform fault and rift valley from bathyscaph and diving saucer. *Science* 190, 108–116.

Auzende, J.-M., Bideau, D., Bonatti, E., Cannat, M., Honnorez, J., Lagabrielle, Y., Malavieille, J., Mamaloukas-Frangoulis, V. & Mével, C., 1989. Direct observation of a section through slow-spreading oceanic crust. *Nature* 337, 726–729.

Baines, A.G., Cheadle, M.J., Dick, H.J.B., Hosford Scheirer, A., John, B.E., Kusznir, N.J. & Matsumoto, T., 2003. A mechanism for generating the anomalous uplift of oceanic core-complexes: Atlantis Bank, SW Indian Ridge. *Geology* 31, 1105–1108.

Baines, A.G., Cheadle, M.J., Dick, H.J.B., Hosford Scheirer, A., John, B.A., Kusznir, N. J. & Matsumoto, T., 2007. Evolution of the Southwest Indian Ridge from 55°45′E to 62°E: Changes in Plate-Boundary Geometry Since 26 Ma. *Geochemistry, Geophysics, Geosystems* 8, Q06022.

Bagherbandi, M., Tenzer, R. Sjöberg, L.E. & Novák, P., 2013. Improved global crustal thickness modeling

based on the VMM isostatic model and non-isostatic gravity correction. *Journal of Geodynamics* 66, 25–37.

Bartsch, C., 2014. *Structural and magnetic investigation of two spreading systems around the Rodriguez Triple Junction with respect to hydrothermal activity*. Naturwissenschaftliche Fakultät, Gottfried Wilhelm Leibniz Universität Hannover, PhD thesis, 237 pp.

Beltenev, V., Ivanov, V., Rozhdestvenskaya, I., Cherkashov, G.,Stepanova, T., Shilov, V., Pertsev, A., Davydov, M., Egorov, I., Melekestseva, I., Narkevsky, E. & Ignatov, V., 2007. A new hydrothermal field at 13°30′N on the Mid-Atlantic Ridge. *InterRidge News* 16, 9–10.

Blackman, D.K. & Collins, J.A., 2010. Lower crustal variability and the crust/mantle transition at the Atlantis Massif oceanic core complex. *Geophysical Research Letters* 37, L24303.

Blackman, D.K., Cann, J.R., Janssen, B. & Smith, D.K., 1998. Origin of extensional core complexes: Evidence from the Mid-Atlantic Ridge at Atlantis Fracture Zone. *Journal of Geophysical Research* 103, 315–333.

Blackman, D.K., Karson, J.A., Kelley, D.S., Cann, J.R., Gretchen L., Früh-Green, G.L., Gee, J.S., Hurst, S.D., John, B.E., Morgan, J., Nooner, S.L., Ross, D.K, Schroeder, T.J. & Williams, E.A., 2002a. Geology of the Atlantis Massif (Mid-Atlantic Ridge, 30°N): Implications for the evolution of an ultramafic oceanic core complex. *Marine Geophysical Research* 23, 443–469.

Blackman, D.K., Lyons, S., Cann, J. & Morgan, J., 2002b. *Morphology of a 9 Myr old oceanic core complex: Mid Atlantic Ridge 30°N, 43°W*. Abstract presented at AGU Fall Meeting, San Francisco, USA.

Blackman, D.K., Karner, G.D. & Searle, R.C., 2008. Three-dimensional structure of oceanic core complexes: Effects on gravity signature and ridge flank morphology, Mid-Atlantic Ridge, 30°N. *Geochemistry,Geophysics,Geosystems* 9, 1–20.

Blackman, D.K., Canales, J.P. & Harding, A., 2009. Geophysical signatures of oceanic core complexes. *Geophysical Journal International* 178, 593–613.

Blackman, D.K., Ildefonse, B., John, B.E., Ohara, Y., Miller, D.J., Abe, N., Abratis, M., Andal, E.S., Andréani,M., Awaji, S., Beard, J.S., Brunelli, D., Charney, A.B., Christie, D.M., Collins, J., Delacour, A.G., Delius, H., Drouin, M., Einaudi, F., Escartín, J., Frost, B.R., Früh-Green, G., Fryer, P.B., Gee, J.S., Godard, M., Grimes, C.B., Halfpenny, A., Hansen, H.-E., Harris, A.C., Tamura, A., Hayman, N.W., Hellebrand, E., Hirose, T., Hirth, J.G., Ishimaru, S., Johnson, K.T.M., Karner, G.D., Linek, M., MacLeod, C.J., Maeda, J., Mason, O.U., McCaig, A.M., Michibayashi, K., Morris, A., Nakagawa, T., Nozaka, T., Rosner, M.,Searle, R.C., Suhr, G., Tominaga, M., von der Handt, A., Yamasaki, T. & Zhao, X., 2011. Drilling constraints on lithospheric accretion and evolution at Atlantis Massif, Mid-Atlantic Ridge 30°N. *Journal of Geophysical Research* 116, B07103.

Bodinier, J.-L. & Godard, M. 2003. *Orogenic, Ophiolitic and Abyssal Peridotites*, [In:] R.W. Carlson (Ed.): Treatise on Geochemistry. Vol. 2: The Mantle and Core. Elsevier, Amsterdam, 103–170.

Bonatti, E., Peyve, A., Kepezhinskas, P., Kurentsova, N., Seyler, M., Skolotnev, S. & Udintsev, G., 1992. Upper mantle heterogeneity below the Mid-Atlantic Ridge, 0°–15°N. *Journal of Geophysical Research* 97, 4461–4476.

Bonatti, E., Ligi, M., Brunelli, D., Cipriani, A., Fabretti, P., Ferrante, V., Gasperini, L. & Ottolini, L., 2003. Mantle thermal pulses below the Mid-Atlantic Ridge and temporal variations in the formation of oceanic lithosphere. *Nature* 423, 499–505.

Buck, R.W., 1988. Flexural rotation of normal faults. *Tectonics* 7, 959–973.

Canales, J.P., Detrick, R.S., Bazin, S., Harding, A.J. & Orcutt, J.A., 1998. Off-axis crustal thickness across and along the East Pacific Rise within the MELT area. *Science* 280, 1218–1221.

Canales, J.P., Detrick, R.S., Toomey, D.R. & Wilcock, W.S.D., 2003. Segment-scale variations in the crustal structure of 150–300 kyr old fast spreading oceanic crust (East Pacific Rise, 8°15′–10°5′N) from wide-angle seismic refraction profiles. *Geophysical Journal International* 152, 766–794.

Canales, J.P., Sohn, R.A. & deMartin, B.J., 2007. Crustal structure of the Trans-Atlantic Geotraverse (TAG) segment (Mid-Atlantic Ridge, 26°10′N): Implications for the nature of hydrothermal circulation and detachment faulting at slow spreading ridges. *Geochemistry, Geophysics, Geosystems* 8, Q08004.

Cann, J.R., Blackman, D.K., Smith, D.K., McAllister, E., Janssen, B., Mello, S., Avgerinos, E., Pascoe, A.R, & Escartín, J., 1997. Corrugated slip surfaces formed at North Atlantic ridge-transform intersections. *Nature* 385, 329–332.

Cannat, M., 1993. Emplacement of mantle rocks in the seafloor at mid-ocean ridges. *Journal of Geophysical Research* 98, 4163–4172.

Cannat, M., 1996. How thick is the magmatic crust at slow spreading oceanic ridges. *Journal of Geophysical Research* 101, 2847–2857.

Cannat, M. & Casey, J.F., 1995. An Ultramafic Lift at the Mid-Atlantic Ridge: Successive Stages of Magmatism in Serpentinized Peridotites from the 15°N Region. *Petrology and Structural Geology* 6, 5–34.

Cannat, M., Mével, C., Maia, M., Deplus, C., Durand, C., Gente, P., Agrinier, P., Belarouchu, A., Dubuisson, G., Humler, E. & Reynolds, J., 1995. Thin crust, ultramafic exposures, and rugged faulting patterns at the Mid-Atlantic Ridge (22°–24°N). *Geology* 23, 49–52.

Cannat, M., Sauter, D., Mendel, V., Ruellan, E., Okino, K., Escartín, J., Combier, V. & Baala, M., 2006. Modes of seafloor generation at a melt-poor ultraslow-spreading ridge. *Geology* 34, 605–608.

Cannat, M., Sauter, D., Escartín, J., Lavier, L. & Picazo, S., 2009. Oceanic corrugated surfaces and the strength of the axial lithosphere at slow spreading ridges. *Earth and Planetary Science Letters* 288, 174–183.

Carlson, R.W., 2003. *Introduction to Volume 2*. [In:] R.W. Carlson (Ed.): Treatise on geochemistry. Vol. 2: The Mantle and Core. Elsevier, Amsterdam, 15–21.

Chamot-Rooke, N., Fournier, M., Petit, C.,Fabbri, O., Huchon, P., Lepvrier C. & Maillot, B., 2008. *Sheba Ridge's*

Oceanic Core Complexes. Abstract presented at EGU General Assembly, Vienna, Austria.

Choi, S.H., Mukasa, S.B. & Shervais, J.W., 2008. Initiation of Franciscan subduction along a large-offset fracture zone: Evidence from mantle peridotites, Stonyford, California. *Geology* 36, 595–598.

Christie, D.M.,West, B.P., Pyle, D.G. & Hanan, B.B., 1998. Chaotic topography, mantle flow and mantle migration in the Australian-Antarctic discordance. *Nature* 394, 637–644.

Coogan, L.A., 2013. *The lower oceanic crust*. Manuscript submitted for publication. 113 pp.

d'Acremont, E., Leroy, S., Maia, M., Patriat, P., Beslier, M.-O., Bellahsen, N., Fournier, M. & Gente, P., 2006. Structure and evolution of the eastern Gulf of Aden: Insights from magnetic and gravity data (Encens-Sheba MD117cruise). *Geophysical Journal International* 165, 786–803.

Dannowski, A., Grevemeyer, I., Ranero, C.R., Ceuleneer, G., Maia, M., Morgan, J.P. & Genteet, P., 2010. Seismic structure of an oceanic core complex at the Mid-Atlantic Ridge, 22°19′N. *Journal of Geophysical Research* 115, 1–15.

deMartin, B.J., Sohn, R.A., Canales, J.P. & Humphris, S.E., 2007. Kinematics and geometry of active detachment faulting beneath the Trans-Atlantic Geotraverse (TAG) hydrothermal field on the Mid-Atlantic Ridge. *Geology* 35, 711–714.

Dick, H.J.B., 1989. *Abyssal peridotites, very slow-spreading ridges and ocean ridge magmatism.* [In:] A.D. Saunders & M.J. Norry (Eds): Magmatism in the Ocean Basins. Geological Society, London, 71–105.

Dick, H.J.B., 2010. *Tale of two core complexes: Contrasting crustal architecture and fault geometries*. Abstract presented at AGU Chapman Conference, Agros, Cyprus.

Dick, H.J.B. & Zhou, H., 2015. Ocean rises are products of variable mantle composition, temperature and focused melting. *Nature Geoscience* 8, 68–74.

Dick, H.J.B., Bryan, W.B. & Thompson, G., 1981. *Low-angle faulting and steady-state emplacement of plutonic rocks at ridge-transform intersections*. [In:] A.R. Ritsema (Ed.): European Seismological Commisssion Meeting and Abstracts. Eos, Transaction American Geophysical Union 62, 406.

Dick H.J.B., Schouten, H., Meyer, P,S., Gallo, D.G., Bergh, H., Tyce, R., Patriat, P., Johnson, K.T.M., Snow, J. & Fisher, A., 1991.Tectonic evolution of the Atlantis II Fracture Zone. [In:] R.P. Von Herzen, P.T. Robinson et al. (Eds): *Proceedings of the Ocean Drilling Program, Scientific Results* 118, 359–398.

Dick H.J.B., Natland J.H., Alt J.C., Bach, W., Bideau, D., Gee, J.S., Haggas, S., Hertogen, J.G.H., Hirth, G., Holm, P.M., Ildefonse, B., Iturrino, G.J., John, B.E., Kelley, D.S., Kikawa, E., Kingdon, A., LeRoux, P.J., Maeda, J., Meyer, P.S., Miller, D.J., Naslund, H.R., Niu, Y.-L. Robinson, P.T., Snow, J., Stephen, R.A., Trimby, P.W., Worm, H.-U. & Yoshinobu, A., 2000. A long in situ section of lower oceanic crust: Results of ODP Leg 176 drilling at the Southwest Indian Ridge. *Earth and Planetary Science Letters* 179, 31–51.

Dick, H.J.B., Arai, S., Hirth, G., John, B.J. & KROO-06 Scientific Party, 2001. A subhorizontal cross-section through the crust mantle boundary at the SW Indian Ridge. *Geophysical Research Abstracts* 3, 794.

Dick, H.J.B., Lin, J. & Schouten, H., 2003. An ultraslow spreading class of ocean ridge. *Nature* 426, 405–412.

Dick, H.J.B., Natland, J.H. & Ildefonse, B., 2006. Past and future impact of deep drilling in the oceanic crust and mantle. *Oceanography* 19, 72–80 .

Dick, H.J.B., Tivey, M.A. & Tucholke, B.E., 2008. Plutonic foundation of a slow-spreading ridge segment: Oceanic core complex at Kane Megamullion, 23°30′N, 45°20′W. *Geochemistry, Geophysics, Geosystems* 9, Q05014.

Dick, H.J.B., Lissenberg, C.J., & Warren, J.M., 2010. Mantle melting, melt transport, and delivery beneath a slow-spreading ridge: The paleo-MAR from 23°15′N to 23°45′N. *Journal of Petrology* 51, 425–467.

Drolia, R.K. & DeMets, C., 2005. Deformation in the diffuse India-Capricorn-Somalia triple junction from a multibeam and magnetic survey of the northern Central Indian Ridge, 3°S–10°S. *Geochemistry, Geophysics, Geosystems* 6, Q09009.

Drouin, M., Godard, M. & Ildefonse, B., 2007. Origin of olivine-rich troctolites from IODP Hole U1309D in the Atlantis Massif (Mid-Atlantic Ridge): petrostructural and geochemical study. *Eos, Transactions American Geophysical Union* 89(53), Fall Meet. Suppl., Abstract T53B-1300.

Drouin, M., Godard, M., Ildefonse, B., Bruguier, O. & Garrido, C.J., 2009. Geochemical and petrographic evidence for magmatic impregnation in the oceanic lithosphere at Atlantis Massif, Mid-Atlantic Ridge (IODP Hole U1309D, 30°N). *Chemical Geology* 264, 71–88.

Drouin, M., Ildefonse, B. & Godard, M., 2010. A microstructural imprint of melt impregnation in slow spreading lithosphere: Olivine-rich troctolites from the Atlantis Massif, Mid-Atlantic Ridge, 30°N, IODP Hole U1309D. *Geochemistry, Geophysics, Geosystems* 11, Q06003.

Dyment, J., Bissessur, D., Bucas, K., Cueff-Gauchard, V., Durand, L., Fouquet, Y., Gaill, F., Gente, P., Hoise, E., Ildefonse, B., Konn, C., Lartaud, F., LeBris, N., Musset, G., Nunes, A., Renard, J., Riou, V., Tasiemski, A., Thibaud, R., Torres, P., Yatheesh, V., Vodjdani, I. & Zbinden, M, 2009. Detailed investigation of hydrothermal site Rainbow, Mid-Atlantic Ridge, 36°13′N: Cruise MoMARDream. *InterRidge News* 18, 22–24.

Dziewonski, A.M. & Anderson, D.L, 1981. Preliminary reference Earth model. *Physics of the Earth and Planetary Interiors* 25, 297–356.

Escartín, J. & M. Cannat, M., 1999. Ultramafic exposures and the gravity signature of the lithosphere near the Fifteen-Twenty Fracture Zones (Mid-Atlantic Ridge, 14–16° N). *Earth and Planetary Science Letters* 171, 411–424.

Escartín, J. & Canales, J.P., 2011. Detachments in oceanic lithosphere: Deformation, magmatism, fluid flow, and ecosystems. *Eos, Transactions American Geophysical Union* 92, 31.

Escartín, J., Mével, C., Mac-Leod, C.J. & McCaig, A.M., 2003. Constraints on deformation conditions and the origin of oceanic detachments: The Mid-Atlantic Ridge core complex at 15°45′N. *Geophysics, Geochemistry, Geosystems* 4, 1067.

Escartín, J., Smith, D.K., Cann, J. Schouten, H., Langmuir, C.H. & Escrig, S., 2008. Central role of detachment faults in accretion of slow-spread oceanic lithosphere. *Nature* 455, 790–794.

Escartín, J., Soule, S.A., Cannat, M., Fornari, D.J., Düşünür, D. & Garcia, R., 2014. Lucky Strike seamount: Implications for the emplacement and rifting of segment-centered volcanoes at slow spreading mid-ocean ridges. *Geochemistry, Geophysics, Geosystems* 15, 4157–4179.

Exon, N., Pandey, D., Gallagher, S., Rajan, S., Coffin, M., Takai, K. & other workshop participants, 2011. *Detailed report on Indian Ocean IODP workshop*. Integrated Ocean Drilling Program, Goa, India, 50 pp.

Fouquet, F., Barriga, F., Charlou, J.L., Elderfield, H., German, C.R., Ondreas, H., Parson, L., Radford-Knoery, J., Relvas, J., Ribeiro, A., Schultz, A., Apprioual, R., Cambon, P., Costa, I., Donval, J.P., Douville, E., Landure, J.Y., Normand, A., Pelle, H., Ponsevera, E., Riches, S., Santana, H. & Stephan, M., 1998. FLORES diving cruise with the Nautile near the Azores – First dives on the Rainbow field: hydrothermal sweater/mantle interaction. *InterRidge News* 7, 24–28.

Fournier, M., Chamot-Rooke, N., Petit, C., Huchon, P., Al-Kathiri, A., Audin, L., Beslier, M.-O., d'Acremont, E., Fabbri, O., Fleury, J.-M. Khanbari, K., Lepvrier, C., Leroy, S., Maillot, B. & Merkouriev S., 2010. Arabia-Somalia plate kinematics, evolution of the Aden-Owen-Carlsberg triple junction, and opening of the Gulf of Aden. *Journal of Geophysical Research* 115, B04102.

Fournier, M., Petit, C., Chamot-Rooke, N., Fabbri, O., Huchon, P., Maillot, B. & Lepvrier, C., 2008. Do ridge–ridge–fault triple junctions exist on Earth? Evidence from the Aden–Owen–Carlsberg junction in the NW Indian Ocean. *Basin Research* 20, 575–590.

Fujimoto, H., Cannat, M., Fujioka, M.K., Gamo, T., German, C., Mével, C., Muench, U., Ohta, S., Oyaizu, M., Parson, L., Searle, R., Sohrin, Y. & T. Yama-ashi, T., 1999. First submersible investigation of mid-ocean ridges in the Indian Ocean. *InterRidge News* 8, 22–24.

Fujiwara, T., Lin, J. Matsumoto, T. Kelemen, P.B. Tucholke, B.E. & Casey, J.F., 2003. Crustal Evolution of the Mid-Atlantic Ridge near the Fifteen-Twenty Fracture Zone in the last 5 Ma. *Geochemistry, Geophysics, Geosystems*. 4(3), 1024.

Gente, P., Thibaud, R., Dyment, J., Fouquet, Y., Ildefonse, B., Hoisé, E., Bissessur, D., Yatheesh, V. & the MOMARDREAM 2008 Scientific Party, 2008. High resolution topography of the Rainbow hydrothermal area, Mid-Atlantic Ridge, 36°14′N. *Eos, Transactions American Geophysical Union* 89(53), Fall Meet. Suppl., Abstract T43B-2027.

Gold, T., 1999. *The Deep Hot Biosphere.* Copernicus, New York, 235 pp.

Gràcia, E., Bideau, D., Hekinian, R., Lagabrielle, Y., & Parson, L. M., 1997. Along-axis magmatic oscillations and exposure of ultramafic rocks in a second-order segment of the Mid-Atlantic Ridge (33° 43′N to 34° 07′N). *Geology* 25, 1059–1062.

Gràcia, E., Charlou, J.L., Radford-Knoery, J. & Parson, L., 2000. Non-transform offsets along the Mid-Atlantic Ridge south of the Azores (38°–34°N): Ultramafic exposures and hosting of hydrothermal vents. *Earth and Planetary Science Letters* 177, 89–103.

Grevemeyer, I., Reston, T.J. & Moeller, S., 2013. Microseismicity of the Mid-Atlantic Ridge at 7°S–8°15′S and at the Logatchev Massif oceanic core complex at 14°40′N–14°50′N. *Geochemistry, Geophysics, Geosystems* 14, 3532–3554.

Han, X., Wu, Z. & Qiu, B., 2012. Morphotectonic characteristics of the northern part of the Carlsberg Ridge near the Owen Fracture Zone and the occurrence of oceanic core complex formation. Abstract presented at *AGU Fall Meeting*, San Francisco, USA.

Hellebrand, E., Snow, J.E., Dick, H.J.B. & Hofmann, H., 2001. Coupled major and trace-element indicators in mid-ocean ridge peridotites. *Nature* 410, 677–681.

Hosford, A., Tivey, M. Matsumoto, T., Dick, H.J.B., Schouten, H. & Kinoshita, H., 2003. Crustal magnetization and accretion at the Southwest Indian Ridge near the Atlantis II fracture zone, 0-25 Ma. *Journal of Geophysical Research* 108, 2169.

Ildefonse, B., Andreani, M., Hoise, E., Ballu, V., Escartín, J., Dyment, J. & Fouquet, Y., 2007. Further geological sampling around the Rainbow hydrothermal site, Mid-Atlantic Ridge. *Eos, Transaction American Geophysical Union* 88(52), Fall Meet. Suppl., Abstract T53B-1306.

Jaroslow, G.E., Hirth, G. & Dick, H.J.B., 1996. Abyssal peridotite mylonites: implications for grain-size sensitive flow and strain localization in the oceanic lithosphere. *Tectonophysics* 256, 17–37.

Jousselin, D., Nicolas, A. & Boudier, F., 1998. Detailed mapping of a mantle diapir below a paleo-spreading center in the Oman ophiolite. *Journal of Geophysical Research* 103, 18153–18170.

Jousselin, D., Nicolas, A., Boudier, F. & Meshi, A., 2013. *High-T detachment shear zone in Mirdita ophiolite (Albania)*. Abstract nr T23F-2656 presented at AGU Fall Meetin, San Francisco, USA.

Kamesh Raju, A.K., Samudrala, K., Drolia, R.K., Amarnath, D., Ramachandran, R. & Mudholkar, A., 2012. Segmentation and morphology of the Central Indian Ridge between 3°S and 11°S, Indian Ocean. *Tectonophysics* 554–557, 114–126.

Karson, J.A., Früh-Green, G.L., Kelley, D.S.,Williams, E.A., Yoerger, D.R. & Jakuba, M., 2006. Detachment shear zone of the Atlantis Massif core complex, Mid-Atlantic Ridge, 30°N. *Geochemistry, Geophysics, Geosystems* 7, Q06016.

Karsten, J., Klein, E., Martinesz, F., Mühe, R., Sturm, M., Coleman, T., Hayasaka, J., Jung, D., Murray, G., Muse, B., Newsom, A., Stewart, M., Tougas, S. & Gallegos, J., 1999. The northern Chile Ridge revealed: Preliminary cruise report of PANORAMA Expedition Leg 04. *InterRidge News* 8, 15–21.

Kelemen, P.B., Hirth, G., Shimizu, N., Spiegelman, M. & Dick, H.J.B., 1997. A review of melt migration processes in the asthenospheric mantle beneath oceanic spreading centers. *Philosophical Transactions of the Royal Society* A 355, 283–318.

Kelley, D.S., Karson, J.A., Blackman, D.K., Fruh-Green, G.L., Butterfield, D.A., Lilley, M.D., Olson, E.J., Schrenk, M.O., Roe, K.K., Lebon, G.T. & Rivizzigno, P., 2001. An off-axis hydrothermal vent field near the Mid-Atlantic Ridge at 30°N. *Nature* 412, 145–149.

Klein, E.M., 2003. *Geochemistry of the Igneous Oceanic Crust.* [In:] R.L. Rudnick (Ed.): Treatise on geochemistry. Vol. 3: The Earth's Crust. Elsevier, Amsterdam, 433–463.

Kostitsyn, Yu.A., Silantyev, S.A., Belousova, E.A., Bortnikov, N.S., Krasnova, E.A. & Cannat, M., 2013. Time of the formation of the oceanic core complex of the hydrothermal field in the Mid-Atlantic Ridge (12°58′N): Evidence from zircon study. *Doklady Earth Sciences*, 447, 1301–1305.

Kumagai, H., Nakamura, K., Toki, T., Morishita, T., Okino, K., Ishibashi, J.I., Tsunogai, U., Kawaguchi, S., Gamo, T., Shibuya, T., Sawaguchi, T., Neo, N., Joshima, M., Sato, T. & Takai, K., 2008. Geological background of the Kairei and Edmond hydrothermal fields along the Central Indian Ridge: Implications of their vent fluids' distinct chemistry. *Geofluids* 8, 239–251.

Lagabrielle, Y., Brovarone, A.V. & Ildefonse, B., 2015. Fossil oceanic core complexes recognized in the blue schist metaophiolites of Western Alps and Corsica. *Earth-Science Reviews* 141, 1–26.

Lavier, L.L., Buck, W.R. & Poliakov, A.N.B, 1999. Self-consistent rolling-hinge model for the evolution of large-offset low-angle normal faults. *Geology* 27, 1127–1130.

Macdonald, K.C., Scheirer, D.S. Carbotte, S. & Fox, P.J, 1993. It's only Topography: Part 2. *GSA Today* 3, 29–35.

MacLeod, C.J., Escartín, J., Banerji, D., Banks, G.J., Gleeson, M., Irving, D.H.B., Lilly, R.M., McCaig, A.M., Niu, Y., Allerton, S. & Smith, D.K., 2002. Direct geological evidence for oceanic detachment faulting : The Mid-Atlantic Ridge , 15°45′N. *Geology* 30, 879–882.

MacLeod, C.J., Searle, R.C., Murton, B.J., Casey, J.F., Mallows, C., Unsworth, S.C., Achenbach, K.L. & Harris, M., 2009. Life cycle of oceanic core complexes. *Earth and Planetary Science Letters* 287, 333–344.

MacLeod, C.J., Carlut, J., Escartín, J., Horen, H. & Morris, A., 2011. Quantitative constraint on footwall rotations at the 15°45′N oceanic core complex, Mid-Atlantic Ridge: Implications for oceanic detachment fault processes. *Geochemistry, Geophysics, Geosystems* 12, Q0AG03.

Maffione, M., Morris, A. & Anderson, M.W., 2013. Recognizing detachment-mode seafloor spreading in the deep geological past. *Scientific Reports* 3, 2336.

Mallows, C. & Searle, R.C., 2012. A geophysical study of oceanic core complexes and surrounding terrain, Mid-Atlantic Ridge 13°N–14°N. *Geochemistry, Geophysics, Geosystems* 13, Q0AG08.

Manatschal, G., Sauter, D., Karpoff, A.M., Masini, E., Mohn, G. & Lagabrielle, Y., 2011. The Chenaillet ophiolite in the French/Italian Alps: an ancient analogue for an oceanic core complex? *Lithos* 124, 169–184.

Martinez, F. & Taylor, B., 2002. Mantle wedge control on back-arc crustal accretion. *Nature* 416, 417–420.

Marty, B. & Yokochi, R., 2006. Water in the Early Earth. *Review in Mineralogy & Geochemistry* 62, 421–450.

McCaig, A., 2010. *Hydrothermal Systems and Detachment Faulting.* Abstract presented at AGU Chapman Conference, Agros, Cyprus.

McCaig, A.M., Cliff, B., Escartín, J., Fallick, A.E. & MacLeod, C.J., 2007. Oceanic detachment faults focus very large volumes of black smoker fluids. *Geology* 35, 935–938.

McCollom, T.M. & Seewald, J.S., 2013. Serpentinites, Hydrogen, and Life. *Elements* 9, 129–134.

Ménez B, Pasini V. & Brunelli, D., 2012. Life in the hydrated suboceanic mantle. *Nature Geoscience* 5,133–137.

Mével, C., Agrinier, P., Cannat, M., Decitre, S., Dappoigny, A., Humler, E., Jendrzejewski, N., Kienast, J.R., Ludden, J., Murton, B., Oufi, O., Rabain, A., Seyler, M. & Tamura, Y., 1997. Sampling the South West Indian Ridge: first results of the EDUL cruise (R/V Marion Dufresne II, August 1997). *InterRidge News* 6, 25–26.

Miller, D.J. & Christensen, N.I, 1997. Seismic velocities of lower crustal and upper mantle rocks from the slow spreading Mid-Atlantic Ridge, south of the Kane transform zone (MARK). [In:] J.A. Karson, M. Cannat, D.J. Miller & D. Elthon (Eds): *Proceedings of the Ocean Drilling Program, Scientific Results* 153, 437–454.

Miranda, J.M., Silva, P.F., Lourenço, N., Henry, B., Costa, R. & Team, S., 2002. Study of the Saldanha massif (MAR, 36°34′N): Constrains from rock magnetic and geophysical data. *Marine Geophysical Research* 23, 299–318.

Mitchell, N., Escartín, J. & Allerton, S., 1998. Detachment Faults at Mid-Ocean Ridges Garner Interest. *Eos, Transaction American Geophysical Union* 79, 127.

Morishita, T., Hara, K., Nakamura, K., Sawaguchi, T., Tamura, A., Arai, S., Okino, K., Takai, K. & Kumagai, H., 2009. Igneous, alteration and exhumation processes recorded in abyssal peridotites and related fault rocks from an oceanic core complex along the Central Indian Ridge. *Journal of Petrology* 50, 1299–1325.

Morris, J.D. & Ryan, J.G., 2003. *Subduction zone processes and implications for changing composition of the upper and lower mantle.* [In:] R.W. Carlson (Ed.): Treatise on geochemistry. Vol. 2: The Mantle and Core. Elsevier, Amsterdam, 451–470.

Mudholkar, A., Kamesh Raju, K.A., Babu, E.V.S.S.K., Sreenivas, B., Vijaya Kumar, T. & Bhaskar Rao, Y.J., 2012. Oceanic core complexes along Carlsberg Ridge. *International Conference: Ridges and Hotspots around the Mascarene Islands*, LUX Island resort, Mauritius.

Nakamura, K., Morishita, T., Bach, W., Klein, F., Hara, K., Okino, K., Takai, K. & Kumagai, H., 2009. Serpentinized olivine-rich gabbroic rocks exposed near the Kairei Hydrothermal Field, Central Indian Ridge: Insights into the origin of the Kairei hydrothermal fluid supporting a unique microbial ecosystem. *Earth and Planetary Science Letters* 280, 128–136.

Nicolas, A., Boudier, F. & Meshi, A., 1999. Slow spreading accretion and mantle denudation in the Miridita ophiolite (Albania). *Journal of Geophysical Research* 104, 15155–15167.

Niu, Y. & Batiza, R., 1994. Magmatic processes at a slow spreading ridge segment: 26°S Mid-Atlantic Ridge, *Journal of Geophysical Research* 99, 19719–19740.

Nuriel, P., Katzir, Y., Abelson, M., Valley, J.W., Matthews, A., Spicuzza, M.J. & Ayalon, A., 2009. Fault-related oceanic serpentinization in the Troodos ophiolite, Cyprus: Implications for a fossil oceanic core complex. *Earth and Planetary Science Letters* 282, 34–46.

Ohara, Y., Yoshida, T., Kato, Y. & Kasuga, S., 2001.Giant megamullion in the Parece Vela backarc basin. *Marine Geophysical Researches* 22, 47–61.

Ohara, Y., Okino, K., Snow, J.E. & KR03-01 Shipboard Scientific Party, 2003a. Preliminary report of Kairei KR03-01 cruise: amagmatic tectonics and lithospheric composition of the Parece Vela Basin. *Interridge News* 12, 27–29.

Ohara, Y., Fujioka, K., Ishii, T. & Yurimoto, H., 2003b. Peridotites and gabbros from the Parece Vela backarc basin: unique tectonic window in an extinct backarc spreading ridge. *Geochemistry, Geophysics, Geosystems* 4, 8611.

Okino, K., Matsuda, K., Christie, D.M., Nogi, Y. & Koizumi, K., 2004. Development of oceanic detachment and asymmetric spreading at the Australian-Antarctic Discordance. *Geochemistry, Geophysics, Geosystems* 5, Q12012.

Palmer, J., Sempere, J.-C., Christie, D.M. & Morgan, J.P., 1993. Morphology and tectonics of the Australian-Antarctic Discordance between 123°E and 128°E. *Marine Geophysical Researches* 15, 121–152.

Palmiotto, C., Corda, L., Ligi, M., Cipriani, A., Dick, H.J.B., Douville, E., Gasperini, L., Montagna, P., Thil, F., Bosetti, A.M., Balestra, B. & Bonatti, E., 2013. Nonvolcanic tectonic islands in ancient and modern oceans. *Geochemistry, Geophysics, Geosystems* 14, 4698–4717.

Parkinson, I.J. & Pearce, J.A., 1998. Peridotites from the Izu-Bonin-Mariana Forearc (ODP Leg 125): evidence for mantle melting and melt-mantle interaction in a supra-subduction zone setting. *Journal of Petrology* 39, 1577–1618.

Pearson, D.G., Canil, D. & Shirey, S.B., 2003. *Mantle Samples Included in Volcanic Rocks: Xenoliths and Diamonds*. [In:] R.W. Carlson (Ed.): Treatise on geochemistry. Vol. 2: The Mantle and Core. Elsevier, Amsterdam, 171–275.

Penrose Conference Participants, 1972. Penrose Field Conference: Ophiolites. *Geotimes* 17, 24–25.

Petersen, S., Kuhn, K., Kuhn, T., Augustin, N., Hekinian, R., Franz L. & Borowski, C., 2009. The geological setting of the ultramafic-hosted Logatchev hydrothermal field (14°45′N, Mid-Atlantic Ridge) and its influence on massive sulfide formation. *Lithos* 112, 40–56.

Planert, L., Flueh, E.R., Tilmann, F., Grevemeyer, I. & Reston, T.J., 2010. Crustal structure of a rifted oceanic core complex and its conjugate side at the MAR at 5°S: Implications for melt extraction during detachment faulting and core complex formation. *Geophysical Journal International* 181, 113–126.

Pyle, D.G., 1993. *Geochemistry of mid-ocean ridge basalt within and surrounding the Australian Antarctic Discordance*. Ph.D. thesis. Oregon State University, 178 pp.

Pyle, D.G., Christie, D.M. & Mahoney, J.J., 1992. Resolving an isotope boundary within the Australian-Antarctic Discordance. *Earth and Planetary Science Letters* 112, 161–178.

Rampone, E., Piccardo, G. B., Vannucci, R. & Bottazzi, P., 1997. Chemistry and origin of trapped melts in ophiolitic peridotites. *Geochimica et Cosmochimica Acta* 41, 4557–4569.

Ranero, C.R. & Reston, T.J., 1999. Detachment faulting at ocean core complexes. *Geology* 27, 983–986.

Reston, T.J., Weinrebe, W., Grevemeyer, I., Flueh, E.R., Mitchell, N.C., Kirstein, L., Kopp, C. & Kopp, H., 2002. A rifted inside corner massif on the Mid-Atlantic Ridge at 5°S. *Earth and Planetary Science Letters* 200, 255–269.

Reston, T.J., Ranero, C.R., Ruoff, O., Perez-Gussinye, M. & Danobeitia, J.J., 2004. Geometry of extensional faults developed at slow-spreading centres from seismic reflection data in the Central Atlantic (Canary Basin). *Geophysical Journal International* 159, 591–606.

Reves-Sohn, R. & Humphris, S., 2004. *Seismicity and fluid flow of the TAG Hydrothermal Mound-4: Cruise report, STAG Leg 4*. Woods Hole Oceanographic Institution, Woods Hole, Massachusetts, 36 pp.

Ribeiro Da Costa, I., Barriga, F.J., Viti, C., Mellini, M. & Wicks, F.J., 2008. Antigorite in deformed serpentinites from the Mid-Atlantic Ridge. *European Journal of Mineralogy* 20, 563–572.

Sato, T., Okino, K. & Kumagai, H. 2009. Magnetic structure of an oceanic core complex at the southernmost Central Indian Ridge: Analysis of shipboard and deep-sea three-component magnetometer data. *Geochemistry, Geophysics, Geosystems*, 10, Q06003.

Schroeder, T. & John, B.E., 2004. Strain localization on an oceanic detachment fault system, Atlantis Massif, 30°N, Mid-Atlantic Ridge. *Geochemistry, Geophysics, Geosystems* 5, Q06015.

Schroeder, T., Cheadle, M.J., Dick, H.J.B., Faul, U., Casey, J.F. & Kelemen, P.B., 2007. Nonvolcanic seafloor spreading and corner-flow rotation accommodated by extensional faulting at 15°N on the Mid-Atlantic Ridge: A structural synthesis of ODP Leg 209. *Geochemistry, Geophysics, Geosystems* 8, Q06015.

Scott, H.P., Hemley, R.J., Mao, H.K., Herschbach, D.R., Fried, L.E., Howard, W.M. & Bastea, S., 2004. Generation of methane in the Earth's mantle: In situ high pressure-temperature measurements of carbonate reduction. *Proceedings of the National Academy of Sciences* 101, 14023–14026.

Searle, R.C. & Bralee, A.V, 2007. Asymmetric generation of oceanic crust at the ultra-slow spreading Southwest Indian Ridge, 64°E, *Geochemistry, Geophysics, Geosystems* 8, Q015015.

Searle, R.C., Cannat, M., Fujioka, K., Mével, C., Fujimoto, H., Bralee, A. & Parson, L., 2003. FUJI Dome: A large detachment fault near 64°E on the very slow-spread-

ing southwest Indian Ridge. *Geochemistry, Geophysics, Geosystems* 4, 9105.

Shipboard Scientific Party, 2003. *Leg 209 Preliminary Report.* Ocean Drilling Program, College Station, Texas, 100 pp.

Shipboard Scientific Party, 2005a. *Expedition 304 Preliminary Report: Oceanic Core Complex Formation, Atlantis Massif.* Integrated Ocean Drill. Program, College Station, Texas, 63 pp.

Shipboard Scientific Party, 2005b. *Expedition 305 Preliminary Report: Oceanic Core Complex Formation, Atlantis Massif.* Integrated Ocean Drill. Program, College Station, Texas, 78 pp.

Skinner, B.J., Porter, S.C. & Park, J., 2004. *Dynamic Earth: An Introduction to Physical Geology*. John Wiley, New Jersey, 630 pp.

Silantyev, S.A., Mironenko, M.V. & Novoselov, A.A., 2009a. Hydrothermal systems in peridotites of slow-spreading mid-oceanic ridges. Modeling phase transitions and material balance: Downwelling limb of a hydrothermal circulation cell. *Petrology*, 17, 138–157.

Silantyev, S.A., Mironenko, M.V. & Novoselov, A.A, 2009b. Hydrothermal systems hosted in peridotites at slow-spreading ridges. Modeling phase transformations and material balance: Upwelling limb of the hydrothermal cell. *Petrology*, 17, 523–536.

Smith, D.K., Cann, J.R. & Escartín, J., 2006. Widespread active detachment faulting and core complex formation near 13° N on the Mid-Atlantic Ridge. *Nature* 442, 440–443.

Smith, D.K., Escartín, J., Schouten, H. & Cann, J.R., 2008. Fault rotation and core complex formation: Significant processes in seafloor formation at slow-spreading mid-ocean ridges (Mid-Atlantic Ridge, 13°–15°N). *Geochemistry, Geophysics, Geosystems* 9, Q03003.

Smith, D.K., Escartín, J., Schouten, H. & Cann, J.R., 2012. Active long-lived faults emerging along slow-spreading mid-ocean ridges. *Oceanography* 25, 94–99.

Smith, D.K., Schouten, H., Dick, H.J.B., Cann, J.R., Salters, V., Marschall, H.R., Ji, F., Yoerger, D., Sanfilippo, A., Parnell-Turner, R., Palmiotto, C., Zheleznov, A., Bai, H., Junkin, W., Urann, B., Dick, S., Sulanowska, M., Lemmond, P. & Curry, S., 2014. Development and evolution of detachment faulting at 50 km of the Mid-Atlantic Ridge near 16.5°N. *Geochemistry, Geophysics, Geosystems* 15, 4692–4711.

Solomon, S.C., Huang, P.Y. & Meinke, L., 1988. The seismic moment budget of slowly spreading ridges. *Nature* 334, 58–60.

Suhr, G., Hellebrand, E., Johnson, K. & Brunelli, D., 2008. Stacked gabbro units and intervening mantle: A detailed look at a section of IODP Leg 305, Hole U1309D. *Geochemistry, Geophysics, Geosystems* 9, Q10007.

Tamura, A., Arai, S., Ishimaru, S. & Andal, E.S., 2008. Petrology and geochemistry of peridotites from IODP Site U1309 at Atlantis Massif, MAR 30°N: micro- and macro-scale melt penetrations into peridotites. *Contributions to Mineralogy and Petrology* 155, 491–509.

Tebbens, S.F., Cande, S.C., Kovacs, L., Parra, J.C., LaBrecque, J.L. & Vergara, H., 1997. The Chile ridge: A tectonic framework. *Journal of Geophysical Research* 102, 12035–12059.

Thatcher, W. & Hill, D.P., 1995. A simple model for fault generated morphology of slow-spreading mid-oceanic ridges. *Journal of Geophysical Research* 100, 561−570.

Tivey, M.A., Schouten, H. & Kleinrock, M.C. 2003. A near-bottom magnetic survey of the Mid-Atlantic Ridge axis at 26°N: Implications for the tectonic evolution of the TAG segment. *Journal of Geophysical Research* 108, 2277.

Tremblay, A., Meshi, A. & Bedard, J.H., 2009. Oceanic core complexes and ancient oceanic lithosphere: Insight from Iapetan and Tethyan ophiolites (Canada and Albania). *Tectonophysics* 473, 36–52.

Tucholke, B.E. & Lin, J., 1994. A geological model for the structure of ridge segments in slow spreading ocean crust. *Journal of Geophysical Research* 99, 11937–11958.

Tucholke, B.E., Lin, J. & Kleinrock, M.C., 1996. Mullions, megamullions, and metamorphic core complexes on the Mid-Atlantic Ridge. *Eos, Transaction American Geophysical Union* 77(46), Fall Meet. Suppl., Abstract F724.

Tucholke, B.E., Lin, J., Kleinrock, M.C., Tivey, M.A., Reed, T.B., Golf, J. & Jaroslow, G.E., 1997. Segmentation and crustal structure of the western Mid-Atlantic Ridge flank, 25°25′–27°10′N and 0–29 m.y. *Journal of Geophysical Research* 102, 203–223.

Tucholke, B.E., Lin, J. & Kleinrock, M.C., 1998. Megamullions and mullion structure defining oceanic metamorphic core complexes on the mid-Atlantic ridge. *Journal of Geophysical Research* 103, 9857–9866.

Tucholke, B.E., Fujioka, K., Ishihara, T., Hirth, G., & Kinoshita, M., 2001. Submersible study of an oceanic megamullion in the central North Atlantic. *Journal of Geophysical Research* 106, 145–161.

Tucholke, B.E., Behn, M.D., Buck, R. & Lin, J., 2008. The role of melt supply in oceanic detachment faulting and formation of megamullions. *Geology* 36, 455–458.

Tucholke, B.E., Humphris, S.E. & Dick, H.J.B., 2013. Cemented mounds and hydrothermal sediments on the detachment surface at Kane Megamullion: A new manifestation of hydrothermal venting. *Geochemistry, Geophysics, Geosystems* 14, 3352–3378.

Wang, W., Chu, F., Zhu, J., Dong, Y., Yu, X., Chen, L. & Li, Z., 2013. Mantle melting beneath the Southwest Indian Ridge: signals from clinopyroxene in abyssal peridotites. *Acta Oceanologica Sinica* 32, 50–59.

White, R.S., McKenzie, D. & O'Nions, R.K., 1992. Oceanic crustal thickness from seismic measurements and rare earth element inversions. *Journal of Geophysical Research* 97, 19683–19715.

Whitney, D.L., Teyssier, C., Rey, P.F. & Buck, W.R., 2013. Continental and oceanic core complexes. *Geological Society of America Bulletin* 125, 273–298.

Wilkinson, J.F.G., 1986. Classification and average chemical compositions of common basalts and andesites. *Journal of Petrology* 27, 31–62.

Wilson, M., 1997. *Igneous Petrogenesis*. Springer, Dordrecht, 466 pp.

Wilson, S., 2010. *Mantle source composition beneath Mid Atlantic Ridge: controls on the development of e-MORB segment and oceanic core complexes*. School of Ocean and

Earth Sciences, University of Southampton, PhD thesis, 392 pp.

Xu, M., Canales, J.P., Tucholke, B.E. & DuBois, D.L., 2009. Heterogeneous seismic velocity structure of the upper lithosphere at Kane oceanic core complex, Mid-Atlantic Ridge. *Geochemistry, Geophysics, Geosystems* 10, Q10001.

Yi, S.B., Oh, C.W., Pak, S.J., Kim, J., & Moon, J.W., 2014. Geochemistry and petrogenesis of mafic-ultramafic rocks from the Central Indian Ridge, latitude 8°–17° S: denudation of mantle harzburgites and gabbroic rocks and compositional variation of basalts. *International Geology Review* 56, 1691–1719.

Yu, Z., Li, J., Liang, Y., Han, X., Zhang, J. & Zhu, L., 2013. Distribution of large-scale detachment faults on mid-ocean ridges in relation to spreading rates. *Acta Oceanologica Sinica*, 12, 109–117.

Zhao, M., Canales, J.P. & Sohn, R.A., 2012. Three-dimensional seismic structure of a Mid-Atlantic Ridge segment characterized by active detachment faulting (Trans-Atlantic Geotraverse, 25°55′N–26°20′N). *Geochemistry, Geophysics, Geosystems* 13, Q0AG13.

Zhao, M., Qui, X., Li, J., Sauter, D., Ruan, A., Chen, J., Cannat, M., Singh, S., Zhang, J., Wu, Z. & Niu, X, 2013. Three-dimensional seismic structure of the Dragon Flag oceanic core complex at the ultraslow spreading Southwest Indian Ridge (49°39′E). *Geochemistry, Geophysics, Geosystems* 14, 4544–4563.

Zhou, H., 2015. Regional geology of active Dragon Hydrothermal Field, Southwest Indian Ridge. *IODP workshop: Indian ocean crust & mantle drilling*, Woods Hole, MA, USA, May 13–16, 2015.

Zhou, H. & Dick, H.J.B., 2013. Thin crust as evidence for depleted mantle supporting the Marion Rise. *Nature* 494, 195–200.

Zonenshain, L.P., Kuzmin, M.I., Lisitsin, A.P., Bogdanov, Y.A. & Baranov, B.V., 1989. Tectonics of the Mid-Atlantic rift valley between the TAG and MARK areas (26–24°N): evidence for vertical tectonism. *Tectonophysics* 159, 1–23.